U.PORTO
FEUP FACULDADE DE ENGENHARIA
UNIVERSIDADE DO PORTO

Design of a Chassis for a Forest Fire Fighting Truck

Jorge Miguel Silva Paiva

Master's Dissertation

FEUP's Supervisor: Prof. José Luís Soares Esteves
FEUP's Co-supervisor: Prof. Marco Paulo Lages Parente
Jacinto's Supervisor: Eng. Jacinto Reis
Jacinto's Supervisor: Eng. Hélder Saleiro

Master in Mechanical Engineering

July 2023

“Um dia vais achar que tens de ir para onde toda a gente vai… Mantém-te original”

Sumol, 2010

Abstract

The dissertation written below is part of the collaboration between the author and the company Jacinto Marques de Oliveira Sucrs, Lda. The company employs over 150 workers and expects this year, 2023, to reach a revenue of more than 40 million Euros. The thesis is part of a new project, from the Innovation department, with the intention to develop a Forest Fire Fighting Vehicle, from scratch, allowing its inhouse production. The truck should have off-road capabilities and a mass of less than 16 tons.

Initially, and before the start of any kind of practical development, a generic context of the project was discussed, along with a review of the situation of forest fires and the history of fire trucks, finalising with an assesemnt of the size and growth of the market for firefighting and rescue vehicles. Next, and after clarifying the entire concept of the truck to be developed, all the documentation applied to the product, such as norms, standards and regulations were gathered and analysed. The EN 1846 standard and the ECE-R29-02 regulation the only ones found concerning the matter. Furthermore, a market study was carried out to understand the differentiating points of the current competition and possible points to consider improving.

Moving on to the practical work carried, an iterative process of chassis proposal designs began, in which every new model involved a discussion with the company's top management. Moreover, the design can be divided into 3 major components, base plan, cabin and axle support. Having the second imposed greater challenges, due to not only the positioning of the engine and transmission, but also the chosen windscreen. Once the final design was achieved, it was subjected to tests, resorting to numerical analysis, to verify structural integrity. The first test is a static test, with a safety coefficient applied, in order to ascertain the structure's capacity to withstand normal loads in running order. A second static test, with the weights of the equipment and occupants, simulating an asymmetric obstacle to confirm the structural capacity to overcome obstructions on the path. And lastly, the three dynamic tests, Test A, B and C, contemplated in the ECE-R29-02 regulations, to certify the cabin in case of an accident.

The final conclusion is that the chassis is capable of passing 2 of the 5 tests, the static test and Test B, the 90° roll-over test. Failing or achieving inconclusive results in the remaining 3, static obstacle transposition, Test A and C, frontal impact and 180° rollover, respecively. In short, a better definition of the components to be equipped and their mounting locations is necessary, as well as a new iteration of the structure with reinforcements in the lower front part and in the first rollbar.

Keywords: Forest Fire Fighting Vehicle; Chassis; EN 1846; ECE-R29-02

Resumo

A dissertação adiante redigida está enquadrada na colaboração entre o autor e a empresa Jacinto Marques de Oliveira Sucrs, Lda. A firma emprega mais de 150 trabalhadores e espera este ano, 2023, atingir uma faturação superior a 40 milhões de Euros. A tese insere-se num novo projeto, do departamento de Inovação, com intuito de desenvolver um VFCI, Veículo Florestal de Combate a Incêndios, de raiz, permitindo um fabrico próprio. O camião deverá ter capacidades fora de estrada e uma massa inferior a 16 toneladas.

Inicialmente, antes do arranque de qualquer tipo de desenvolvimento prático, fez-se um contexto geral do projeto, fez-se uma revisão ao estado dos incêndios florestais e à história dos camiões de bombeiros, passando ainda pela dimensão e crescimento do mercado de veículos de socorro e de combate a incêndio. De seguida, e após um esclarecimento de todo o conceito do camião a desenvolver, fez-se uma recolha e análise de toda a documentação aplicada ao produto, normas, standards e regulamentação. Recolheu-se a norma EN1846 e o regulamento ECE-R29-02. Para além demais foi feito um estudo do mercado para compreender os pontos diferenciadores da atual concorrência e eventuais pontos a considerar melhorar.

Passando ao trabalho prático desenvolvido, iniciou-se um processo iterativo de desenho de propostas do chassis, no qual todos os novos modelos implicavam uma discussão com a gestão de topo da empresa. O desenho pode ser dividido em 3 grandes componentes, plano base, cabine e apoio dos eixos. Tendo o segundo imposto maiores desafios, devido tanto ao posicionamento do motor e transmissão, como ao para-brisas escolhido. Após alcançado o desenho final, este foi sujeito a testes, recorrendo a simulação numérica, para verificar a integridade estrutural. O primeiro teste é um teste estático, com um coeficiente de segurança aplicado, com o intuito de apurar a capacidade da estrutura de aguentar com as cargas normais em ordem de marcha. Um segundo teste estático, com os pesos dos equipamentos e ocupantes, a simular um desnível assimétrico para confirmar a capacidade estrutural de transpor obstáculos. E por último os 3 testes dinâmicos, Teste A, B e C, comtemplados na regulamentação ECE-R29-02, para a certificação da cabine em caso de acidente.

No final conclui-se que o chassis é capaz de passar em 2 dos 5 testes, teste estático e Teste B, capotamento a 90° do veículo. Falhando ou tendo sido atingidos resultados inconclusivos nos restantes 3, transposição de obstáculo, Teste A e C, impacto frontal e capotamento a 180°, respetivamente. Em suma, será necessária uma melhor definição dos componentes a equipar e os seus locais de montagem, assim como uma nova iteração da estrutura com reforços na parte frontal inferior e no primeiro *rollbar*.

Palavras-chave: Veículos florestais de combate a incendio; Chassis; EN1846; ECE-R29-02

Acknowledgements

The work developed during this last 4.5 months would never be possible without the presence, help and support of some individuals. For this reason, I would like to express my appreciation and gratitude towards them.

First and foremost, I have to express my gratitude towards Eng. Jacinto Reis for the opportunity and for the challenge to be part of such big and dauting project to tackle without any experience, and to Professor José Luís Esteves for joining along with such spontaneous invitation. Additionally, a special thanks needs to be addressed to Eng. Hélder Saleiro for all the time spent together developing the numerous iterations of the chassis and to Professor Marco Parente for the availability and all the hasty and direct Abaqus explanations.

The second group of people that I would like to acknowledge are my friends, those that were strangers on my first day at FEUP but stand to turn out to be the most important ones on this past 5 years. To those who were always around, always by my side, supporting me and sharing so many time together, a big shout out. And on a slightly more limited reference, thanks Manuel Henrique and Afonso Hora for our continuous battle during the Master's.

Finally, to my parents, to my grandparents, godparents and cousins, to those that are family, even though not being it, my sincere respect and thankfulness. I would never be the person I grew up to be and the engineer I am graduating in, without all the things that you taught me, the support and constant encouragement.

Lastly, the most special and particular mention belongs to my grandmother, my personal teacher and the person that taught me to be curious and enthusiastic about my studies. She has been a crucial part of my academic journey since the 1st day of school, molding my attitude towards learning and enjoying.

Contents

List of Figures

List of Tables

1 Introduction

1.1 Context of the thesis

The following thesis was carried within the scope of the Aeronautic and Vehicle Structures specialization of the Mechanical Engineering Mater's study program at Faculdade de Engenharia da Universidade do Porto, FEUP. The thesis is part of a collaboration between Jacinto Marques de Oliveira Sucrs Lda and the author, with Eng. Hélder Saleiro as the mentor at Jacinto and Professor José Luís Esteves as FEUP's advisor. The work to be carried out is the initial part of a R&D, Research and Development, project of the company that aims to develop a forest fire fighting truck with a vehicle mass below 16 t with all terrain capability, i. e., in compliance with NP EN 1846-1, the Portuguese Norm of the European Standard, EN 1846-1 [1], a forest firefighting appliance – EN 1846 – M – 3. More specifically, it will focus on the design, using 3D CAD software, Autodesk Inventor Professional 2024, and study, resorting to Finite Element Method, FEM, analysis, through SIMULIA Abaqus 2020 software, of a chassis for a new under development forest fire fighting middle weight vehicle.

The future steps of the project, until the truck is ready for prototyping, include the development of the firefighting hydraulic system, electric scheme, equipment allocation, etc. In sum, the vehicle, when fully developed, is intended to stand out from the competition and allow for the establishment of a dedicated assembly line exclusively for the manufacture of this model.

1.2 Jacinto Marques de Oliveira Sucrs, Lda and the R&D department

Jacinto Marques de Oliveira Sucrs, Lda, for now on abbreviated to Jacinto, is a Portuguese company that roots back to 1954. It started with manual pumps to draw water from wells. After the 1974, 25th of April Carnation Revolution, the business had a shift towards prefabricated metal houses, becoming the main product flag for the following 20 years. A new strategical shift occurred after, transforming the focus of production for what the company is now known for. Counting now with more than 30 years of experience building all types of fire fighting vehicles, it represents more than 85% of today's business revenue. Jacinto's production site is situated in Esmoriz and employs over 150 workers. It exports vehicles for all around the world, being Chile its biggest frequent customer and Romania's 2021, 200 vehicles, purchase agreement, the largest order ever placed. In 2022 Jacinto's revenue accounted to more than 30 million Euros, confirming the upward trend from previous years. This year, 2023, the value is expected to rise to more than 40 million.

In 2019, the firm showcased its first electric prototype, the Eco Camões, shown in Figure 1. The presented model was the first completely electric, unmanned capable, up to 1 km remote controlled, fire fighting vehicle in the world with 300 km range and ensuring 4h of continuous pump operation. Hence allowing for operator risk free missions with zero emissions. This fire truck, with its 10 000 l water, 1 200 l foam and 250 kg dry chemical powder holding capacities, can be operated under both EN 1846 [1, 2, 3], NFPA 414 [4] and ICAO [5] standards, making it possible to classify as an ARFF, aircraft rescue and firefighting truck [6].

Figure 1. Eco Camões [7].

After Eco Camões project, in 2020, General Manager Eng. Jacinto Reis proposed establishing a R&D department. It was then created in 2021 and includes at the moment 2 dedicated engineers, 1 electrical and 1 mechanical, complemented by a top management team composed by 3 other elements from 2 other departments, Project and Quality along with General Manager Eng. Jacinto Reis.

Another initiative of the R&D department was an electrical urban environment firefighting truck. With an estimated 400 km range, 2 000 l +200 l of water and foam tank capacities, the vehicle has adjustable chassis in height and also offers the possibility to transform its 1+1+4 passengers' cabin into an operational command center, thanks to its movable seats [6].

Lastly, there are two other projects for innovative equipment and technology under development. The first one, a forest firefighting equipment, is a self-supporting nozzle system, which can throw water over a flame front. It aims to reduce the direct exposure of firefighters to the flames and can be easily explained as a nozzle attached to a flying drone. Finally, with the objective of entering in the 3 billion euros forest management and other linked activities and its resources exploration market, Jacinto has announced the E-Forest project. It aims to empower forest management teams with efficient means in the biomass control and wildfire prevention fields and attenuate the consequences of the aging of rural population. More explicitly, it consists in the employment of autonomous modular robots to regulate forest environments [6].

1.3 Objectives

The project, where this thesis is included, is in an early stage, mostly conceptual, with no palpable or digital resources still in existence at the time the dissertation started to be composed. Thus, the initial step is the research, gathering and revision of all required and applicable documentation to the product to be developed, such as regulations and European standards. It will be followed by a forest fire truck market review and the subsequent comparison with the envisioned requirements of the future machine.

Next, and moving on to the core practical goal, the focus is the development of a new chassis for a forest fire truck. This includes the design of it, respecting the requirements imposed by the top management team of Jacinto and to the norms and standards applicable to these types of vehicles, and a following stress and strain study resorting to FEM analysis to verify the integrity of the designed chassis. Ultimately, along with the proof that the structure can stand the normal working weight load of equipment and extinguishing agent, the cab shall, also, be certifiable according to the UN regulation ECE-R29-02 [8]. Thus, FEM simulation of the required tests will be performed.

1.4 Thesis structure

The thesis is divided into 5 chapters.

The preset section introduces the context of the thesis, giving an overview of the project and the company where it is included, along with the description of the objectives set.

The second chapter showcases the environment of the project, contextualizing the problem of wildfires along with its past and anticipated future evolution, in addition to the history of fire trucks and the current dimension and growth of the market.

On the third section not only the conceptual idea of the vehicle will be described, but also the applicable standards and regulations will be presented and the current solutions made available on the market by other players reviewed.

The more extensive chapter, the fourth, is where all the design process is showed and explained. It starts by revealing the 3 drawing periods of the chassis with the corresponding justification to the choices made and ends with the validation of the product, resorting to FEM analysis. 2 static analysis will be carried, along with 3 dynamic studies according to ECE-R29-02. Material properties, modelling, meshing, and assembly loading conditions of each FEM job is also demonstrated.

The last portion of the thesis is where the final conclusions are drawn and the possible future work is proposed.

2 The context of forest fires and firefighting vehicles

2.1 Wildfires and present panorama

A wildfire is an ungoverned fire that breaks out, when minimum fuel and ignition conditions are met, in a wilderness or rural setting like shrublands, forests, meadows or prairies. The source of ignition can be natural, for instance a lightning strike, or due to human responsibility, either negligent or intentional. Moreover, the abundance, continuity and fuel moisture are also driving factors. High temperatures and lack of precipitation decreases the humidity content on fuel, hence increasing the fire outbreak risk. Natural fire regimes and occurrences can be beneficial for the ecosystem by boosting biodiversity and conservating landscapes. However, it can rapidly reach the tipping point depending on the rise of intensity and frequency of the events, resulting in vast negative results for both environment and society [9, 10].

The wildfire season in Europe spans from the beginning of June until the end of September. The quantity of damaged terrain, in the last 4 years, is on a raising trend for most of the countries of central and eastern Europe. For instance, Romania was in the top place of the European Union, EU, podium for burnt area in 2019 and 2020 and experienced territorial losses greater than 10 times the values of the average destroyed area of the corresponding previous decade in 2019, 2020 and 2022 [11]. Still, it is the southern, Mediterranean, part of Europe that is particularly prone to wildfires, due to its dry and hot summers, as proven by Figure 2. The EUMED5 (France, Greece, Italy, Portugal and Spain) countries represent, on average more than 85% of the total annual burnt area on European Economic Area, EEA [11]. Furthermore, it is plausible to conclude that is the Iberian Peninsula that is more consistently afflicted and with greater extensiveness by wildfires.

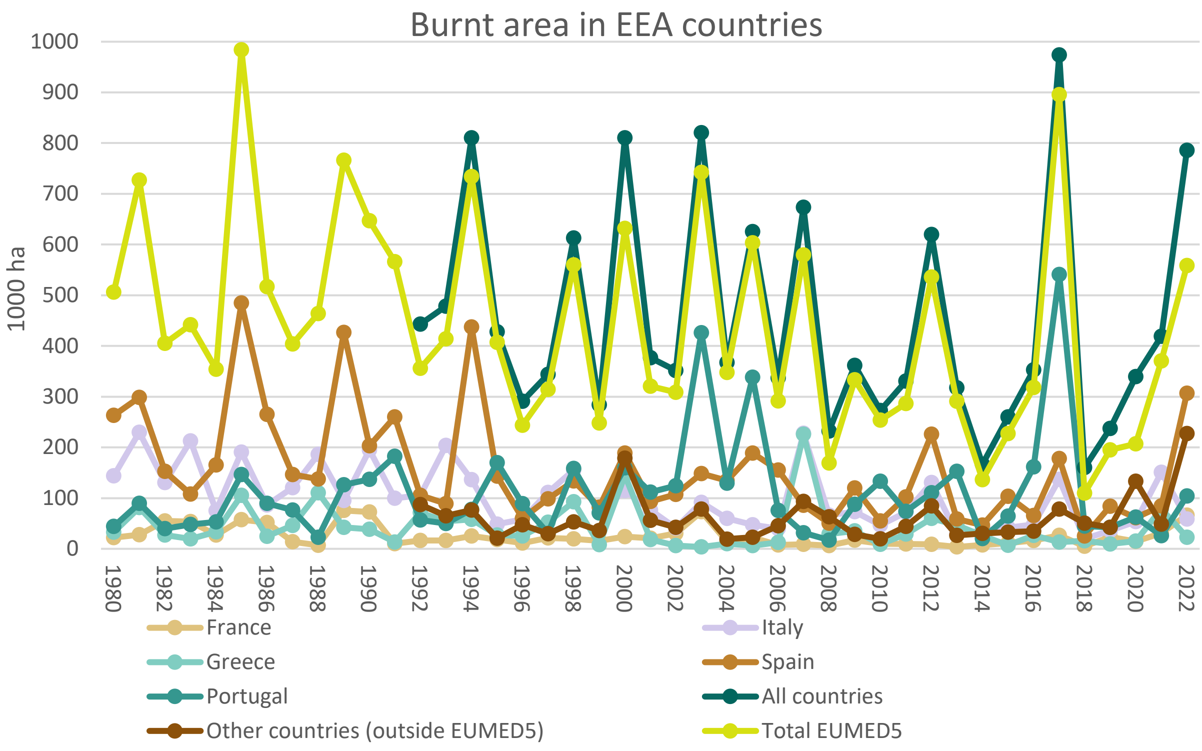

Figure 2. Burnt Area in EEA members (1980-2022), data until 2019 from [12] and 2020-2022 from [11].[1]

The most western country of Europe is regularly one of the most affected European nations by flames. In Portugal, the annual critical period of wildfires is decreed to be between the 1st of July to the 30th of September by the 2nd Article of the Portuguese law n. º 76/2017, *Lei n.º 76/2017, de 17 de agosto*. Additionally, the government can extend this period in exceptional situations, as in 2017, the most devastating year for the Portuguese forest. When more than 100 people passed away and more than 500 000 ha were burnt, more than 5 times the mean area of the prior decade [9, 13]. The majority of the events were triggered by human hand, 28% intentionally and 48% by negligence for the 10-year period between 2012 and 2021 [14]. Last year, 2022, the total real area that got burned by rural and forest fires was 110 007 ha, 12% less than the average value calculated for homologues periods of the previous 10 years (values until 15th of October of 2022 from the last ICNF provisional report [14]). Moreover, the real value of burnt area was lower than the ICNF's computed expected value, 152 478 ha. Value that is achieved by dividing the DSR index[2] into classes and giving an average value of burnt area to each one of them according to the historical data of the last years.

2.2 Climate change and the increase of wildfires

Even though, last year, Portugal had a lower value than the expectable scorched area based on the meteorological conditions experienced and also lower than the average, this was not the case for the rest of the continent. With a total sum of more than 750 000 ha, the 27 EU countries had their land burned almost 3 times more than the average, 260 000 ha, between 2006-2021. These wildfires (plus UK's) led to an estimated emission of 6.4 megatons during the three

[1] Data outside EUMED5 is only available after 1992.

[2] More information available in ANNEX A.

critical summer months, the highest amount since 2007. Similar record high was registered in the Eurasia region, highest value of emissions since 2010, and overall, most regions experienced values near the highest of the past years [15]. These values are worrisome, as the pollution generated by fires can be far more harmful than the industrial emissions, due to its composition of particulates, carbon monoxide, and other pollutants [16]. Consequently, this pollution is also responsible for the worsening and speeding of the current climate change and temperature rise.

Central Spain and southwest France, last year, had, respectively, their live fuel moisture content below historical minimums for 45% and 27% of the three critical summer months' days. Furthermore, lightning strikes, associated to dry thunderstorms, were the most relevant source of ignition for the more extreme fire. These summer thunderstorms are regularly related to thermal lows eventually developing after sustained anticyclonic conditions driving abnormally high temperatures [10]. Altogether and although, Copernicus Atmosphere Monitoring Service, CAMS, data is not capable of directly connect climate change with the observed increase in frequency of high-intensity wildfires. It can be partially associated with the recent, more regular, experienced extreme climate events such as long-term drought conditions or hot and dry stormy weather conditions [16, 17]. These adverse occasions and the global rise of temperature not only impact on the humidity content of fuel but also the quantity, continuity, structure and composition of the it, thus weather can also be considered as a driver of biomass accumulation [9].

Figure 3 materializes the mean change of seasonal proportion of days per decade in each fire danger classes, as estimated from the derivation of Fire Weather Index, FWI[3], obtained from both [9] and [18] reviews' for 3 future scenarios of raise of global temperature. Being these possibilities, from better to worse, 1.5º C, 2º C and 3º C of worldwide temperature increase. On all studies reviewed, fire danger and season length follow a similar trend on all 3 thermal hypotheses. The temperature increment leads to an enhancement of the consequences. The Balkans, part of Turkey, Greece and Italy, France and the Iberian Peninsula present the most noticeable shift in fire danger classes in Europe. A decrease in the frequency of lower risk classes and an increase on the most severe and critical ones. The season length is also expected to extend significatively on all these regions. In contrast, the Baltic and central eastern zone of Europe show an increase in the number of days with safer FWI values. This shall lead to a decrease in frequency of more warning and fire susceptible days, yet this is only expected to be observable in the case of intermediate FWI rated days, as more dangerous FWI values shall have its frequency maintained. Nonetheless, as experienced in the past, the predictions show that it is the southwest zone of the European continent that will have its fire regime most affected due to global warming. A relative increase of 2 to 4% per decade in the average seasonal fire danger ranges is expected in the Iberian Peninsula, reaching 7% in the case of the south part of France. On top of a wider range in fire danger classes, the mean value of it, as measured by the SSR, is also projected to increase by 3-7% per decade in the Mediterranean area. Finally, the southern European zone is expected to have its fire seasons increased in 3 to 4 days every 10 years [9, 18].

[3] Full explanation of the FWI System in ANNEX A.

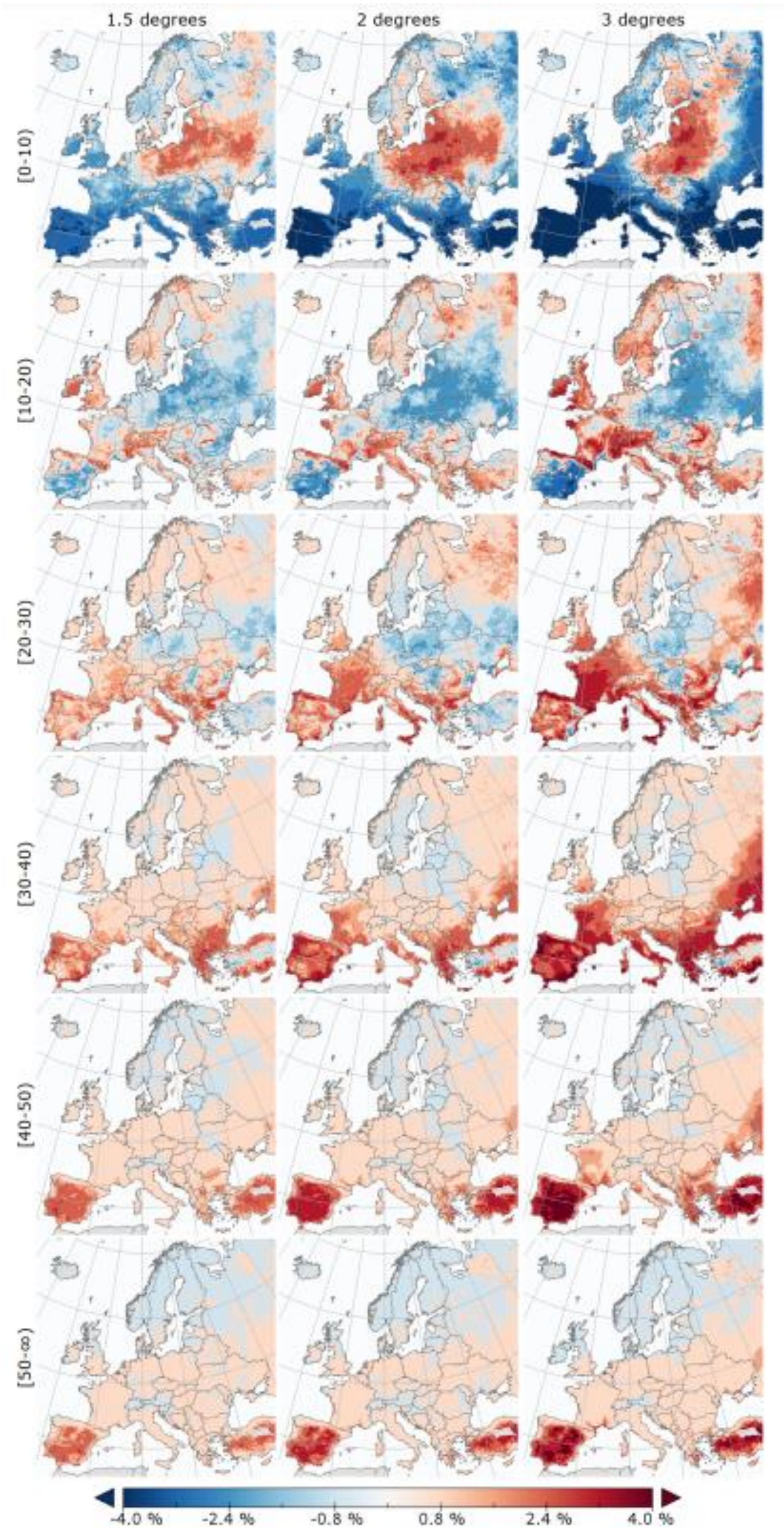

Figure 3. Comparison of the average variation per decade of the daily FWI classes between the control period (1971 2000) untill 2100 [18].

2.3 History of fire fighting vehicles

Fire is part of the human life since its discovery and mastery in the Homo Erectus era. Water was also discovered, since the earliest years of human existence, to be able to control and extinguish fire by cooling and smothering it. During the XVIII century, studies were focused on quick extinguishing solutions, innumerous methods and mixtures were created. Yet all used the same principal, to combat fire directly to its main source, the fire zone burning more violently and generating more heat. Dr. Van Marum, in 1794, through experimentation found that plain water was capable of doing just the same, empirically, extinguishing a 7.3 x 7 x 4.3 m (Length x Width x Height) house fill with twisted straw, wood shavings, and cotton soaked in turpentine in around 4 minutes and using just 5 buckets of water [19]. Even though with an extensive evolution, this firefighting technique and the usage of water still are the common standard practice today.

The extinguishing time efficiency of such method is highly dependent on the time between ignition and intervention, or on the size and concentration of the fire. In other words, the readiness and timeliness of reaction to a fire is a major condition for its development and extinguishment. Therefore, innumerous were the inventions and recommendations since this era to cope with such conditions, from the mounting of water tanks on top of every edifice to the suggestion that every city should have at least one fire engine and to the development of fire sprinklers, similar to the widely used today, or the first hand held fire extinguishers [19, 20]. Nonetheless, fire engines can be considered as inventions from the 2nd century before Christ, thanks an engineer named Ctesibiu, also called the father of pneumatics. He invented the first water pump, Figure 4, with identical principles as today's pumps work [19].

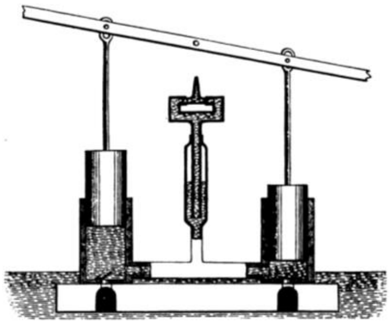

Figure 4. Ctesibiu's Engine II century B.C. [19].

Curiously, only near the end of XVI century, are there the first records of the usage of transportable water squirters/pumps. In 1578, the Englishman, Cyprian Lucar published on *Théâtre des Instruments* the sketch and description of the wheeled squirter seen in Figure 5 a). Later, in 1615, Decaus illustrated his German engine presented in Figure 5 b), in his book *Forcible Movements*, with a flexible pipe and mounted on a sledge as its mean of transportation [19].

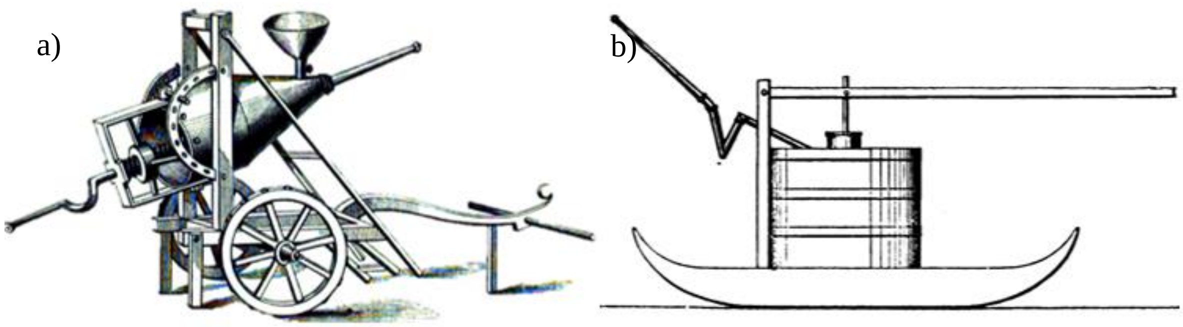

Figure 5. a) Lucar's movable Squirter [19]; b) Sledged Decaus's engine [19].

Many other developments were introduced and great improvements could be found on the used fire engines in the end of the 18^{th} century and until mid of the 19^{th}. From the introduction of bigger pump barrels with greater bore and stroke to the optimization of the levering system and operation with more personal, manual fire engines were capable of injecting water more than 18 meters vertically and more than 30 m horizontally and achieving steady flows of 600 litres per minute [19].

Not only is water extensively useful in liquid form, but also as a gas. Evidence show that steam power was known soon after Ctesbiu's inventions. Heron of Alexandria has described the *Aeolipile*, a steam turbine, in a manuscript, *Spiritalia seu Pneumatica*, in the I century. It consisted in steam ejected tangentially from nozzles coupled to a heated pivoted ball reservoir causing it to spin [21, 22]. Latter and distinct applications followed, from an organ powered by air escaping from compression by heated water to Leonardo da Vinci's steam powered cannon, *Architonnerre*. Yet, it was only in the XVII century that gas and liquid form were put to work together [21, 22, 23].

In 1606, Spanish mining administrator, Jerínimo de Ayanz y Beaumont patented the first steam powered machine that could display water from mines. Still, the credits for the first water pump driven by steam are not given to him, but to the English engineer Thomas Savery, that only 92 years later, in 1698 patented his creation. His model worked with a combination of vacuum, created by condensing steam, and steam pressure, applying Denis Papin, French physicist, theories of cylinder and piston steam engines. According to Savery, it could elevate water 80 feet high (more than 20 meters), yet, to do so it needed pressures of 35 psi (2.4 bar), this led to a pump prone to boiler explosions. Even with the volatility of the pressure vessels and the limitation of placement to be 25 feet high from the water, the design was not discarded and in 1711, another Englishman, Thomas Newcomen releases a new iteration of the pump. The redesigned system required lesser steam pressure accumulation, nearly paired to the atmospheric one, solving the problem of the blow ups of components. This allowed for the engine to be upscaled and to be used for pumping out water from mines, drain wetlands, supplying water to settlements and even power mills and factories. Newcomen product thrived without competition for 60 years, until James Watt come up with a model that fixed the disappointing efficiency of that pump. Watt used a separate condenser to eliminate the wasted energy on the process of heating and colling the steam cylinder of Newcomen engine, allowing to reduce the thermal stresses caused by this cycle as the cylinder was hot all the time. Watt's pump model boosted by the financial aid and futuristic vision of another English engineer, Matthew Boulton, was crucial in the Industrial Revolution. Watt-Boulton engine was applied in all sorts of manufacturing and producing units and after some iterations along with different engine configurations even transports were using steam as the power source [22, 23, 24].

One of the latest applications of steam driven equipment was the steam fire engine. England was the birthplace of them, in 1830 by the hand of John Braithwaite and Ericsson, Figure 6. It was horse-drawn and 20 minutes after lighting the fire, the pump was capable of dumping 150 gallons of water per minute (567.8 l/min) or 30 to 40 tons of water per hour to heights between 80 to 100 feet (24.4 m to 30.5 m). Further iterations followed and a better and more powerful model was delivered to the King of Prussia, 2 years later, to protect the public buildings of Berlin. Still, this was not enough to establish a stable and growing industry around it and for more than 20 years, no production took place in the country and adoption in the continent was slow [19, 23].

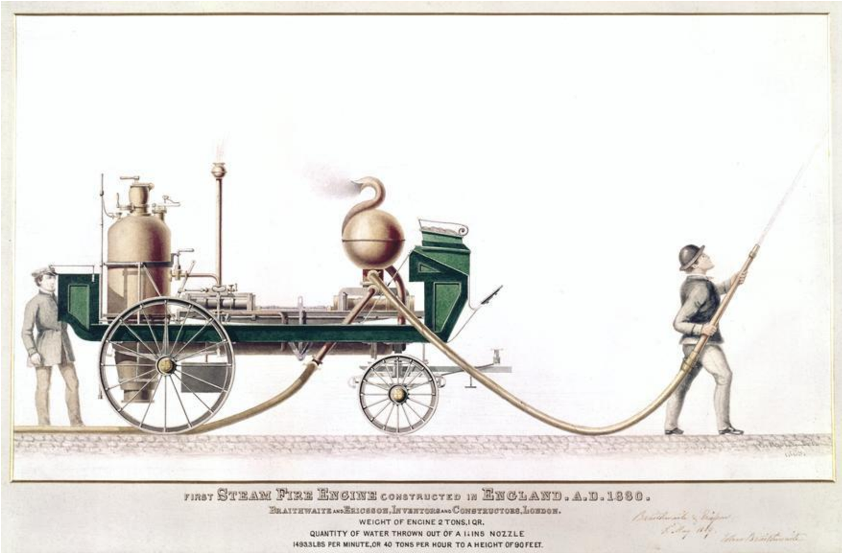

Figure 6. First steam fire engine, John Braithwaite and Ericsson [25].

The transition to the new source of power to feed pumps, on the other side of the Atlantic Ocean, started in 1841 with the fire engine capable of self-propelling built by Paul Rapsey Hodge, Figure 7. This fire apparatus was very similar to the Braithwaite's invention, yet it was capable of making the technology get traction among fire brigades more easily. New iterations on the following years by Novelty Works, The Messrs. Latta, of Cincinnati and Amoskeag Company and the introduction of rotary engines and pumps were capable of lowering substantially the idling time, to 4 minutes, before steam pressure was enough to operate. Therefore, creating the perfect environment to make this machinery thrive [19, 23].

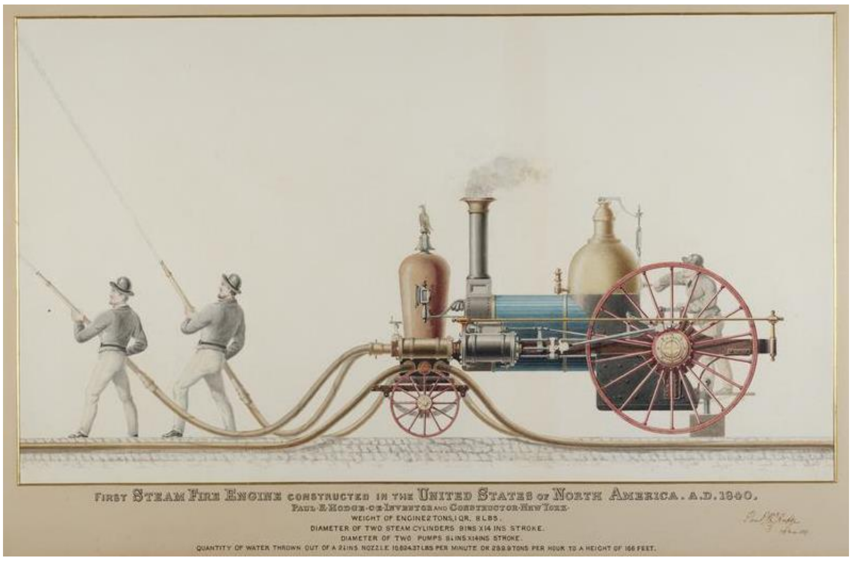

Figure 7. First American Steam Engine, Paul Rapsey Hodge [26].

After 1852, Europe's construction and acceptance among fire brigades started to progressively increase, even with pumps that were not much better than Braithwaite's engine. Being only in July of 1860 that the first land steam fire apparatus used by the London Fire Engine Establishment [19, 23]. It was also on the same decade, 1867, that Portugal embraced the new era of firefighting. With the arrival of steam fire engines to the territory, landlords and property owners were obligated to install fire hydrants. On top of that, it was around the same time that the precursor of the well-known *Magirus* ladder, *escada Fernandes*, appeared and the first attempts to establish the national firefighter's association, Liga dos Bombeiros Portugueses, occurred [27, 28].

The present epoch of firefighting with internal combustion engines as the driving source harks back to 1888 and to Gottlieb Daimler's patent application for the first gasoline-powered fire-fighting pump. This new technology assured the elimination of the fire destroying idly watch that steam powered engines demanded and diminished the time needed to reach the emergency location. Even with the amendment of the usage of gas-powered extinguishers, under carbonic acid pressure, that fire brigades employed for the initial 15-20 minutes period of firefighting, the full fire combat power was not reached. Until the invention of the high-speed centrifugal pump, in 1909, Daimler preached, showcased and tested his innovation to change the popular scepticism, similarly to what happened with the steam fire apparatus. By December of 1906, the first engine was delivered and put into operation by SAG, Süddeutsche Automobilfabrik Gaggenau. Soon and with the enhanced use of the engine output and the capability of pumping the water jet twice as high into the air, originated from the new type of pump, the trend started to pick up. In 1907, the German company, by then already integrated in Benz & Cie., focused in its "Grunewald Type" model, a self-propelled fire-fighting pump capable to reach 35 km/h and climb 16% gradients [29, 30]. By 1937, the first diesel-powered fire truck, Figure 8, was assembled, in the United States of America, by Stutz Fire Apparatus Company, resorting to a 175 horsepower inline 6 cylinder Cummins engine [31].

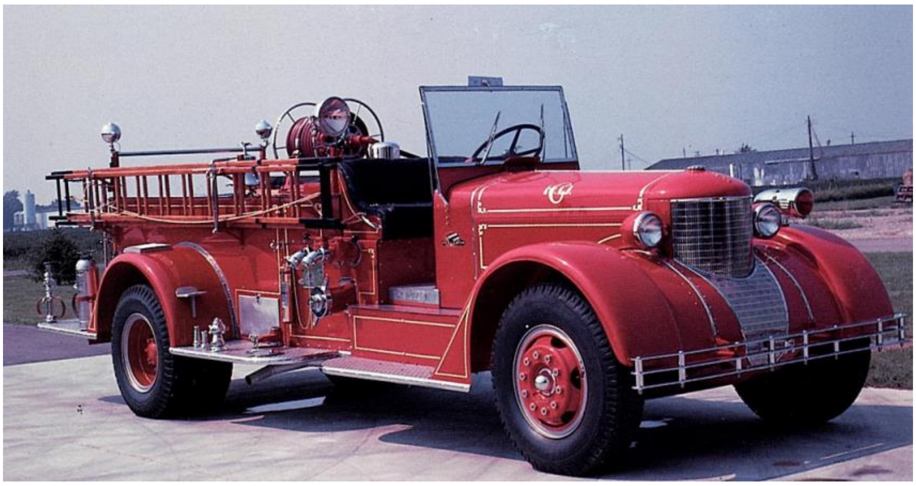

Figure 8. 1st Diesel Fire Truck [31].

Although, diesel represents nowadays practically the only energy source of fire engines, electrification is the next trend. A technology that is not new among this application but that did not get traction by the time, as in 1885, American electrical engineer, Schuyler Wheeler received his patent to the first electric fire engine [32]. It was proven that the efficiency of these was far superior to steam apparatus and that was possible to manufacture self-propelled fire engines resorting only to batteries. Cincinnati and Paris Fire Brigades were two that purchased these types of vehicles. Still, the operational range and costs were limiting for the settlement of this energy source [33, 34, 35]. 135 years later, technology has evolved and, companies are investing big in the transition, with hydrogen being also another energetic source possibility.

2.4 Fire truck market

The fire truck market was valued, in 2021, by Maximize Market Research [36], at 5.54 billion US dollars. It was projected, by the same firm, to reach 7.35 billion USD, by 2030, corresponding to a 3.6% Compound Annual Growth Rates, CAGR. Mordor Intelligence [37], evaluated the market to a size of 5.50 billion USD in 2023 and estimated a 6.83% CAGR, achieving the value of 8.21 billion USD by 2028. Finally, Market Research Future [38] sized the market to 5.8 billion USD by 2021 and forecasted a growth from 6.1 to 8.2 billion USD between 2022 and 2030, presenting a 4.5% CAGR. According to MMR[4] [36], the North America region represents around half of the pie, Europe nearly 25%, following Asia, the Middle East and Africa, taking South America the smallest slice.

When focusing on the European region, the market was valued at 2.15 billion in 2021 by MI[5] [39], that projected a 2.36% CAGR for the period of 2022 to 2027. Eurostat [40] reported that, in 2020, the EU members spent a total of 32.9 billion euros on fire protection services, accounting to 0.5% of the general government total expenditure. Romania was the EU country with the highest percentual expenditure. By consulting Eurostat's database [41], it is concludable that the value has been firmly growing and that the Eastern European countries have been the ones allocating percentual more resources to the cause in the last years.

The global fire truck industry is considered by MMR[4] [36] as a highly consolidated market, being dominated by a limited number of players. Yet, this does not correlate when it comes to the old continent, where there is a big number of manufacturers, creating a competitive market. Furthermore, the trend is that big money is being invested in R&D projects of vehicle electrification and incorporation of advanced digital technologies along with the formation of partnerships between fire truck manufacturers and original truck suppliers to boost revenues and competencies [36, 39].

In sum, and regardless of a more conservative or optimistic economic review and forecast, the market is growing at a steady and solid rate. Most European countries are buying and renovating their firefighting fleets, mainly boosted by the increasing number fire hazards, such as the changing FWI annual profiles, as presented in 2.2. Thus, it can be expected that a new well designed and operational forest vehicle can be succeeded.

[4] Maximize Market Research;

[5] Mordor Intelligence.

3 Project – Rhino Truck

3.1 The project

The project under development at Jacinto is originated from an idea of CEO Eng. Jacinto Oliveira and General Manager Eng. Jacinto Reis. The concept is to build a product that can be mostly built in house and challenge the forest fire fighting appliance market with a unprecedent top-shelf solution. It can even be noted that alternative power sources to the standard diesel, such as electrification and hydrogen, were considered, yet quickly discarded due to technology limitation. Furthermore, the production goal of the project is the designation of a dedicated assembly line exclusively to this new model, achieving on the first 2 years a total production of 50 units and doubling it to 100 vehicles/year on the subsequent years.

Regarding the vehicle itself, on top of a greater water carrying capacity than similar sized vehicles, it will include a narrower body, shorter wheelbase and lower center of gravity than the current available options on the market to ensure an enhanced manoeuvrability. More specifically, the automotive shall be able to carry 5 500 l of extinguishing agent and all firefighting equipment stored as low as possible. In order to further create a more capable machine, the vehicle is also intended to be equipped with an independent suspension system and an all-wheel driving system.

Additionally, and aiming to reduce costs of manufacturing, the top management team has decided that the windscreen to be used will be the same as employed on Jacinto's narrow 2.5 m ARFF truck, Lusitano.

Figure 9. Lusitano ARFF truck [7].

Table 1 presents the initial requisites imposed to the project by the top management team.

Table 1. Initial measurable requisites of the vehicle

Requisite	**Symbol**	**Value**
Dimensions LxWxH (mm)		5 900 x 2 200 x 2 700
Weight (kg)		15 000
Wheelbase (mm)		3 100
Tank capacity (l)		5 500
Approach angle (º)	α	35
Departure angle (º)	β	35
Crew cab (driver+members)		1+4

Complementary to the list of initial requisites of the project, CEO, Eng. Jacinto Oliveira made available his conceptual sketch, as presented in Figure 10. The desired manufacturing approach for the model was also transmitted as described later in this section.

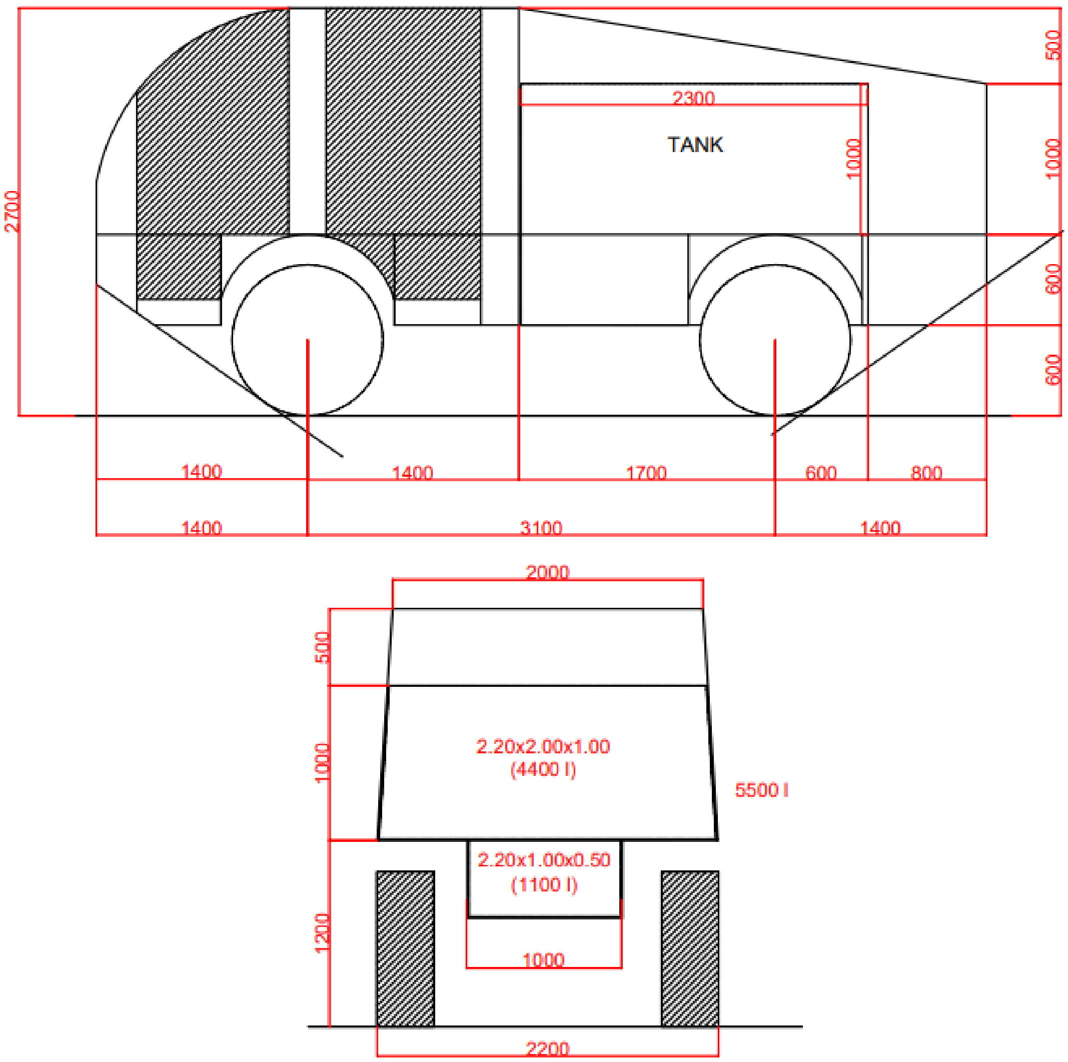

Figure 10. Eng. Jacinto Oliveira's Rhino Truck concept.

Furthermore, the envisioned equipment: engine, water pump and transmission system for the future model were also defined. This is detrimental during the designing process to allocate the required space for each component and know the weight of each one of them. Table 2 presents the respective information. Noticeable, the passengers' seats shall, preferably, be SCBA[6] ready.

Table 2. Permanent components for Rhino Truck

Component	Make	General dimensions L x W x H (mm)	Mass (kg)
Engine	Cummins B6.7	-	522
Transmission	Allison 3000	850 x 500 x 800	300
Transfer Case	ADS TC820	575 x 450 x 620	135
Axles (front/rear)	ADS AX75	-	935/881
Water pump	Jacinto	-	170
Water tank	Jacinto	2 300 x 3 000 x 1 000	≈ 6 000

Additionally, the construction philosophy to be employed on the superstructure is of a rigid monobloc tubular structure. The component responsible for supporting all the loads induced in the vehicle will be designed as one: cabin, power unit and transmission holder, axle mounts, equipment bays, storage boxes and water tank platform will all be projected as a single structure. One consequence of the approach to be used is the limitation in access to engine, transmission and other moving parts that are regularly reachable with just the movement of the truck's cab. In this case the normal tilting mechanism will not exist and these equipment will need to be maintained and intervened from the inside of the crew compartment resorting to a hatch in the middle of the cockpit. Ideally this opening can work as the workbench commonly present in this type of vehicle, where communication equipment and other small portable gear rests.

Moreover, the water reservoir will have a vertical T configuration to allow for a reduction of the height of the center of gravity, CG. Therefore, the tank will need to be holed through so that engine power can be delivered mechanically from the PTO, power take-off, port on the transmission to the rear fitted water pump by a shaft. Expectably, the circular opening will be placed on the bottom part of the water storage.

As a final remark, preferably, all employed beam sections should be from the currently Jacinto's list of used sections, and for any exposed beams, the section should be circular, since this is the common practice among all forest fire fighting trucks manufactured by the company, as shown in Figure 11. Likeminded, two back storage boxes must exist, one each side of the vehicle, even if small.

[6] Self-contained breathing apparatus.

Figure 11. Jacinto's VFCI[7] example [7].

3.2 Applicable standards and regulations

The design and project of this future Jacinto’s model, along with meeting the initial internal objectives, it must respect the requirements imposed by the norms, standards and regulations applicable to these vehicles. To ensure that all relevant documentation was consulted, LTA – Laboratório de Tecnologia Automóvel, a Portuguese homologation and approval entity, was inquired and legislation made available on IMT, I.P. – Instituto da Mobilidade e dos Transportes, the Portuguese transport and mobility regulator, website [42] was review.

Finally, the standard and legislation to be met are the EN 1846 [1, 2, 3] regarding the type and purpose of the vehicle and the ECE-R29-02 [8] in respect to the integrity and safety of the truck cabin.

3.2.1 EN 1846-2 [2]

The first document is divided in 3 parts and imposes some design and performance requirements based on the definition of the category, class and type of the firefighting and rescue service vehicle that the same norm defines. Part 1 [1] has all the definitions and nomenclature needed, part 2 [2] presents the common requirements for firefighting and rescue service vehicles, while part 3 [3] refers to all the permanently installed equipment and dangers. The important information for the designing phase is contemplated in part 2.

In the case of the forest firefighting appliance being developed, a medium (M) mass class and all terrain category (category 3), the static, dynamic and geometric requisites imposed are shown in Table 3.

[7] VFCI – Veículo florestal de combate a incêndio, stands for forest fire fighting truck

Table 3. EN 1846-2 [2] dynamic and geometric requirements

Requisite	Symbol	Value
Approach angle (º)	α	≥35
Departure angle (º)	β	≥35
Angle of slope (º)	γ	≥30
Ground clearance (m)	d	≥0.40
Ground clearance under axle (m)	h	≥0.30
Cross-axle capability (m)	c	≥0.25
Turning circle between walls (m)	D	≤18
Static tilt angle (º)	δ	≥25+3[8]
Gradient capability (º)	P	≥27

Since the model being developed includes a compartment for 3 crew members, EN 1846-2 [2] further requires a minimum of 1 400 mm width at elbow height, with each seating position having more than 400 mm in breadth. Moreover, the cabin shall also have at least 1 050 mm of height between the seats and the interior roof and 450±50 mm from the top of the seat to the cab surface, and more than 300 mm of space in front of the seating bench for the legs and feet, respecting the scheme in Figure 12.

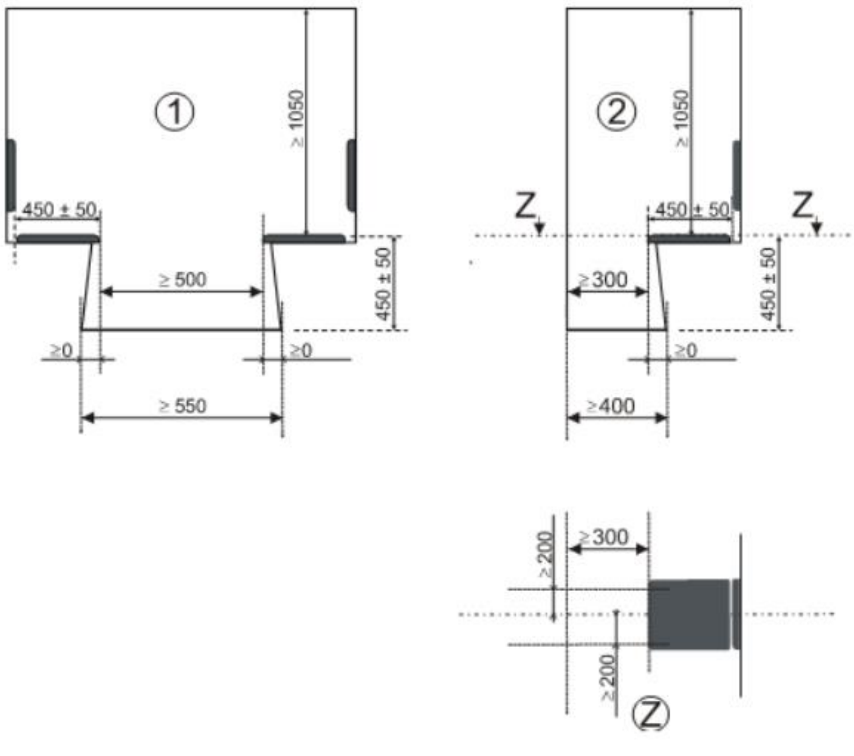

Figure 12. Dimensional limits of crew compartment [2].

[8] Due to the existence of the water tank.

The access to this cabin partition is also regulated. The door shall have a minimum height of 1 050 mm and 600 mm of width, as presented in Figure 13, and be able to open 80º and remain in the fully opened position. Even though the limits are applied solely to the crew compartment, the access to the driver's cab will be designed respecting similar dimensions.

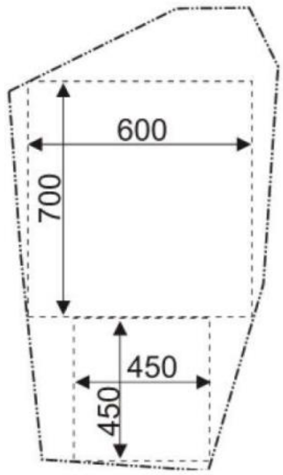

Figure 13. Dimensional limits for the crew compartment door [2].

Similarly, limits are imposed to step accesses, as in Figure 14. The steps shall have a width greater than 300 mm and while the first step shall be at no more than 600 mm from the floor, *d*, between steps the distance shall be inferior to 450 mm, *b*. Lastly, all steps shall be visible from a top vertical position and have a depth, *a*, greater than 150 mm, a horizontal distance between consecutive steps minor than 150 mm and an α angle lower than 85º.

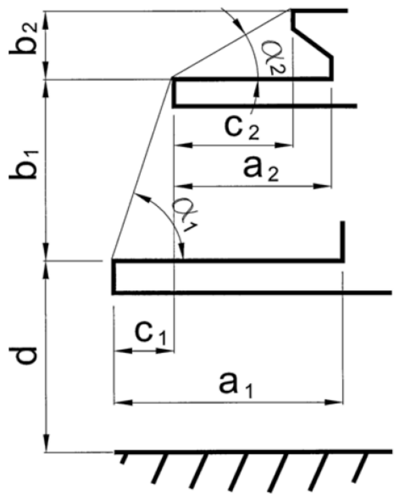

Figure 14. Dimensional limits for step accesses to the cabin [2].

Along with these enforced measurements and characteristics, EN 1846-2 [2] also mandates other aspects and features of the vehicle, such as access to the roof and working platforms. Yet, these will not be mentioned as they do not affect directly the current structural design of the chassis.

3.2.2 ECE-R29-02 [8]

This second regulation ensures the safety of the occupants of the cabin of N[9] class vehicles, thus applicable to the future model. To certify a cab, 3 tests, Test A, B and C, need to be conducted and results shall demonstrate that no structure, chassis or equipment, enters into contact with the occupants. The first one, Test A, assesses the resistance of the cabin to frontal impact accidents. While the second one, Test B, aims to evaluate the resistance of a cab in a 90° rollover accident with subsequent impact, which noticeably, is only necessary for N vehicles with a gross mass over 7.5 t, hereby applicable to the future truck under development. Finally, Test C, intendeds to check the protection of both driver and passengers in case of a 180° rollover accident. Additionally, the tests can be performed on the same or separately on individual cabs at manufacturer's choice. Besides, Test A requires that the cab is installed on a vehicle, Test B and C allow for the cabin to also be coupled to separate frame if wished. In both cases, measures should be taken to guarantee that the body undertesting does not shift appreciably. Furthermore, the physical tests can be substituted by computer simulation, resorting to FEM software, or calculations of the strength of the component parts of the cab or by any other means that can satisfy the Technical Service, ensuring that the cabin will not suffer any dangerous deformation to the occupants if subjected to the conditions of the tests. Thus, during testing, the steering mechanism, steering wheel, instrument panel and seats shall be equipped and the engine or an equivalent thereto model in mass, dimensions and mountings shall also be fitted.

The parameters and conditions for each test are described below:

Test A – Front impact test

Figure 15 is the scheme of the first test. A real impact scenario is reproduced resorting to a 2 500 x 800 mm (*b* x *h*) rigid flat impactor with a minimum, evenly distributed, mass of 1 500 kg hanged by two beams spaced not less than 1 000 mm apart, *f*, and longer than 3 500 mm from the CG of the impactor to the axis of rotation of the apparatus, *L*. The strike shall be inflected to the foremost part of the vehicle and the face of the pendulum shall hit horizontally and parallel to the median longitudinal plane of the vehicle. The impact energy shall be of 55 kJ for N vehicles with gross mass greater than 7.5 t (29.4 kJ for lighter trucks than 7.5 t).

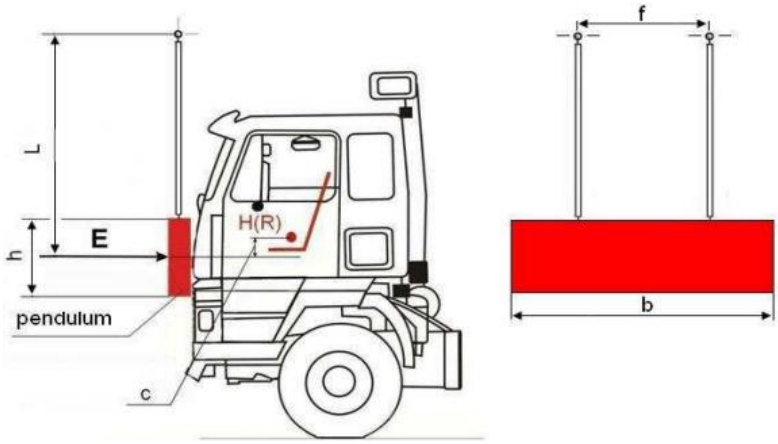

Figure 15. Front impact test (Test A) [8].

[9] Power-driven vehicles having at least four wheels and used for the carriage of goods, according to European Union Regulation EU 2018/858.

Test B – Front pillar impact test

Figure 16 is the scheme of the second test. Homologous to the previous test, a swinging pendulum will hit the cab. In this case, the contact happens in the A-pillars, midway between the lower and the upper windscreen border. Besides, the impactor is cylindrical with a diameter, *d*, of 600 ± 50 mm and a width, *b*, of at least 2 500 mm, ensuring the overlap of the full width of both A-pillars, also the minimum mass is of 1 000 kg. Finally, the impact shall generate an energy of 29.4 kJ.

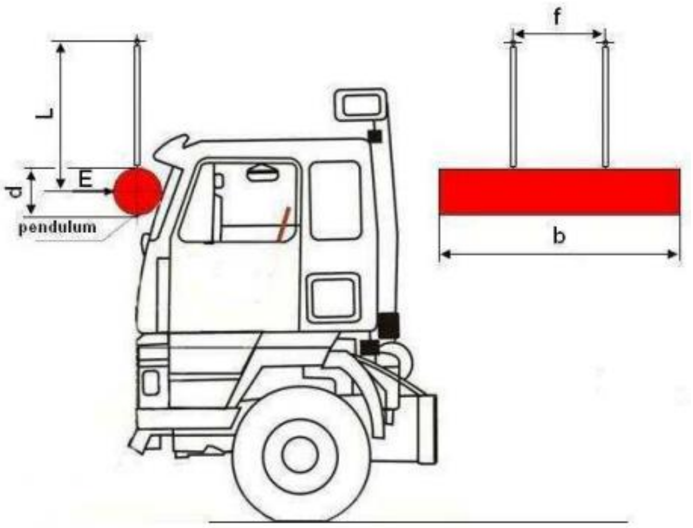

Figure 16. Front pillar impact test (Test B) [8].

Test C – Roof strength test

Figure 17 is the scheme of the third test. Test C consists of 2 loadings prescribed to the cab. A dynamic pre-loading, P_1, simulating an initial hit during a 180° rollover, followed by a compressive loading on the roof, P_2.

The first load, P_1, is a strike of a flat rectangular rigid impactor with an even distributed mass of at least 1 500 kg and size capable of covering all top side of the cabin. The collision shall occur at a 20° angle with the medium longitudinal plane of the cab. The angle can be achieved by either by tilting the structure undertest or the striking body. Nonetheless, the impact energy needs to be equal or higher than 17.6 kJ.

The following load, P_2, is prescribed by a flat rectangular loading device made of steel and with even distributed mass. The mechanism shall load the cab parallel to the x-y plane and moving parallel to the vertical axis of the chassis. Furthermore, the surface shall cover the whole top area of the roof and the static load shall correspond to the maximum mass authorized for the front axle(s), to a limit of 98 kN.

Noticeably, the initial condition, P_1, is only mandatory for trucks over 7.5 t.

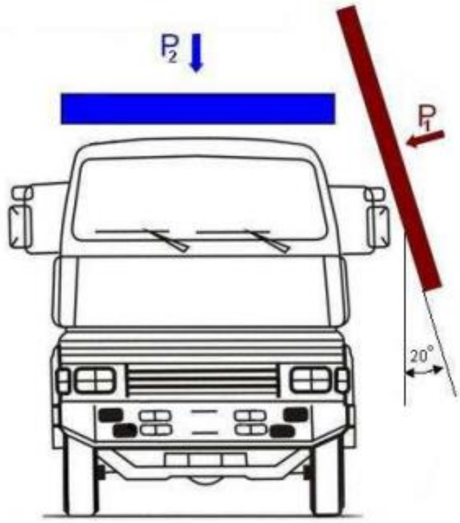

Figure 17. Roof strength test (Test C) [8].

In sum, cab manufacturers shall be able to confirm that no penetration of the structure and equipment into the survival space and consequential collision with driver and/or passengers occurs for the 3 testing conditions by any experimental, numerical or satisfactory analytical method to achieve certification. It is within the scope of this certification that part of the structural integrity of the developed chassis will be tested and tried to be validated.

3.3 Other market players

As just presented, the project aims to introduce in the market a unique solution. To guarantee such single characteristics, an extensive national and international market research will be conducted.

Portugal, alongside Jacinto, has Tuga Fire and Luís Figueiredo as producers of these type of machines. Noticeably, it was not possible to gather useful information from Luís Figueiredo's Forest fire fighting trucks' as there is no public data sheets available.

Tuga Fire is a spinoff born in 2015 derived from the Portuguese firm Camionantunes, Comércios de Viaturas, LDA, an importer and seller of all types of trucks since the 70's. The young company buys and transforms mostly used trucks. Nevertheless, it has already delivered some good-looking models to national and international fire brigades. Table 4, showcases some of the characteristics of the vehicles equipped with the structures produced by Tuga Fire. The Mercedes Unimog model presented, Figure 18, has interesting dimensions but lacks on water storage capacity. While the Scania's and Renault's models, Figure 19 and Figure 20 respectively, are too wide and longer to face Jacinto's proposed product.

It shall be noted that according to the data sheets published by Tuga Fire [43], apart from the Unimog, Figure 18, none of the other models can be considered a forest fire fighting vehicle due to inferior approach angles than what EN 1846-2 [2] states, 35º, moreover some information is missing as it was not published.

Table 4. TugaFire models specifications [43]

Model	General dimensions L x W x H (mm)	Wheelbase (mm)	Tank size (l)	Weight (kg)	Additional features	Figure
Unimog U435F	5 470 x 2 200 x 2 540	3 250	1 700	-	-	Figure 18
Scania P360	6 544 x 2 500 x 3 046	-	4 000 + 300 for self protection	-	-	Figure 19
Renault Midlum 300 CCR	6 700 x 2 400 x 3 100	-	3 300 + 300 for self protection	-	-	Figure 20

Figure 18. TugaFire Unimog U435F [43].

Figure 19. TugaFire Scania P360 [43].

Figure 20. TugaFire Renault Midland 300 CCR [43].

Overall, no direct competition to the future Jacinto's model was found in Portugal. When it comes to the global market, the list of manufactures is lingering, yet, if exclusive American operators are discarded, Rosenbauer and Magirus are one the most resonant companies.

Rosenbauer is an Austrian fire fighting vehicles and equipment manufacturer with more than 150 years of experience in the market. It is the world's leader on systems for firefighting and disaster protection, even having a subsidiary exclusively for the American market due to the norm discrepancies compared to the rest. Forest fires are also one of the areas the company proudly invests in. The latest R&D developments count with 3 different fire trucks. The first one is a Mercedes UNIMOG U5023 4x4 based, Figure 21, the second with a Tatra Force T815 4x4 starting vehicle, Figure 22, and the last one built on a Renault D14 HIGH K R4x4 280, Figure 23. On Table 5 the most significant specifications of the priorly stated trucks are shown. Additionally, all the models are equipped with polypropylene, PP, tanks. The current aluminium Jacinto's standard extinguishing agent tanks are presumably heavier options. Finally, it is concludable that the last two solutions presented by the Austrian builder are the most relevant competitors facing the product to be developed for Jacinto. Tatra due to its independent suspension system and increased manoeuvrability thanks to the all-wheel steering and Renault since it has a comparable wheelbase. Nevertheless, all models presented fall short when their capacity of transporting crew members is analysed.

Table 5. Rosenbauer models specifications [44]

Model	General dimensions L x W x H (mm)	Wheelbase (mm)	Tank size (l)	Weight (kg)	Additional features	Figure
Unimog U5023	7 150 x 2 550 x 3 200	3 850	3 800	14 500	150 l foaming agent tank	Figure 21
Tatra Force T815	7 600 x 2 550 x 3 000	4 182	4 200	18 000	150 l foaming agent tank All wheel steering Independent suspension	Figure 22
Renault D14 HIGH K	6 900 x 2 500 x 3 400	3 350	3 000+ 500 for self protection	14 000	100 l foaming agent tank	Figure 23

Figure 21. Rosenbauer UNIMOG U5023 4x4 [44].

Figure 22. Rosenbauer Tatra Force T815 4x4 [44].

Figure 23. Rosenbauer Renault D14 HIGH K R4x4 280 [44].

Another big and old player on the market is Magirus. Founded in the XIX century, as Rosenbauer, this German manufacturer is best known for its, worldwide revolutionary invention, the turntable ladder. Still, the company also produces for all the range of applications of firefighting and rescuing trucks. Since it is part of the Iveco group, the produced vehicles are predominantly based upon Iveco platforms. Nonetheless, Table 6 shows some of the latest solutions created and manufactured by the company. The first Magirus product, Figure 24, even though having a narrow body it still has a greater wheelbase than the aimed for Jacinto's truck. Furthermore, it can be classified as an outlier, as the maximum weight is limited to 7.2 t and the tank capacity is considerably lower than the desired one. Still, this model deserves to be kept in mind as it can present the limitations that such dimensions can bring. The second Magirus' vehicle, Figure 25, even though bigger in every aspect than aimed to the project, falls short in tank capacity. Lastly, the 6000 l tanker, Figure 26, although with a different purpose and lacking passenger space, presents itself with relatively comparable dimensions and water reservoir volumetry as the future product under development.

Table 6. Magirus models specifications [45, 46]

Model	General dimensions L x W x H (mm)	Wheelbase (mm)	Tank size (l)	Weight (kg)	Additional features	Figure
Iveco double cab CCFL	5 730 x 2 080 x 2 650	3 480	1 800	7 200	-	Figure 24
Iveco HLF 2-WB 3000	7 200 x 2 550 x 3 300	3 690	3 300	15 000	-	Figure 25
Iveco CCF 6000	6 750 x 2 500 x 3 000	3 460	6 000	15 700	-	Figure 26
FireBull	8 228 x 3 077 x 3 395	-	9 000 + 1 000 foam	30 000	Track driven Rotates on own axis	Figure 27

Figure 24. Magirus Iveco double cab CCFL [45].

Figure 25. Magirus Iveco HLF 2-WB 3000 [45].

Figure 26. Magirus Iveco CCF 6000 [45].

As a final complementary remark, new, distinct and extremely oriented forest fire fighting vehicles and equipment have already been shown on international fairs, such as Interschutz, the biggest international fire combat and surveillance related fair in the world. Most of the presented solutions have been small/medium robots and drones with remote control. On the other hand, Magirus opted for a different approach, developing a caterpillar driven prototype, Figure 27, based on the PowerBully18T.

Figure 27. Magirus FireBull [45].

Even though, very far from what was initially assumed as the optimal solution, this Magirus product is interesting to analyse, as PowerBully offers a smaller version, PowerBully 12C, 6 036 x 2 590 x 3 005 mm, and smaller carrying capacity, totalizing ≈26 t, that could be, eventually, transformed and adapted for the same purpose of the current under progress project. The 12C model is capable of a fording depth of 1 300 mm and achieve ground pressure inferior to 0.44 kg/cm^2. Yet, the incompatibilities with the requirements start immediately with the mobility of the machine. It would not be capable of achieving speeds greater than 14.5km/h, it would only be offroad worthy and the desired, EN 1846-2 [2] meeting, loss of stability, approach and departure angles not respected [47]. Hence, this solution is to be discarded as it would fit better a project for peat and swamped environments.

Other global smaller manufacturers, like Iturri [48] and Ziegler [49], and R&D projects were consulted but no significant product specifications or technologies stood out from what was already covered.

In sum, to achieve the desired initial requisites, Table 1, the truck chassis and tank need to be designed and manufactured by Jacinto integrally, as the desired dimensions are so distinguished from what is currently available on the market and due to the unique shape that the reservoir will have to have.

4 Chassis – Rhino Truck

4.1 Iterations of the chassis

The design process will be developed as an iterative design with regular discussion between top management team and the author along with Eng. Hélder Saleiro. The drawing progression is carried using Autodesk Inventor Professional 2024 CAD software, and can be divided into 3 big stages: base plane, the cab and the axle support that will be further detailed next.

4.1.1 Base plane

The base plane is the part of the structure where the tank and the floor of the cab sits. It works as the foundations, absorbing most of the overall stresses, of the chassis and it is from where the rest of the frame arises. Besides, it is also the base component of regular manufactured sub-chassis of Jacinto's regular transformed vehicles, thus substantial expertise, experience and previous solutions are available to consult. Regularly this element is fastened to the stringers of OEM trucks and it is responsible for withstanding the weight load of the water tank and equipment. Yet, in the present model, the stringers will need to be integrated directly on this core element. Thus, the beams assigned for the job are S275 steel square 100 x 4 mm hollow sections, the stiffer available section on Jacinto's catalogue, and run along most of the length of the chassis. When it comes to the transversal stiffening, the design of chassis is extremely limited at this height as the engine and transmission, water tank and pump are inserted, respectively from the front to the back (left to the right of Figure 28), in the three central openings. To tackle this restrains, transversal mechanical bearing capacity should come from a lower section, as will be described in 4.1.3.

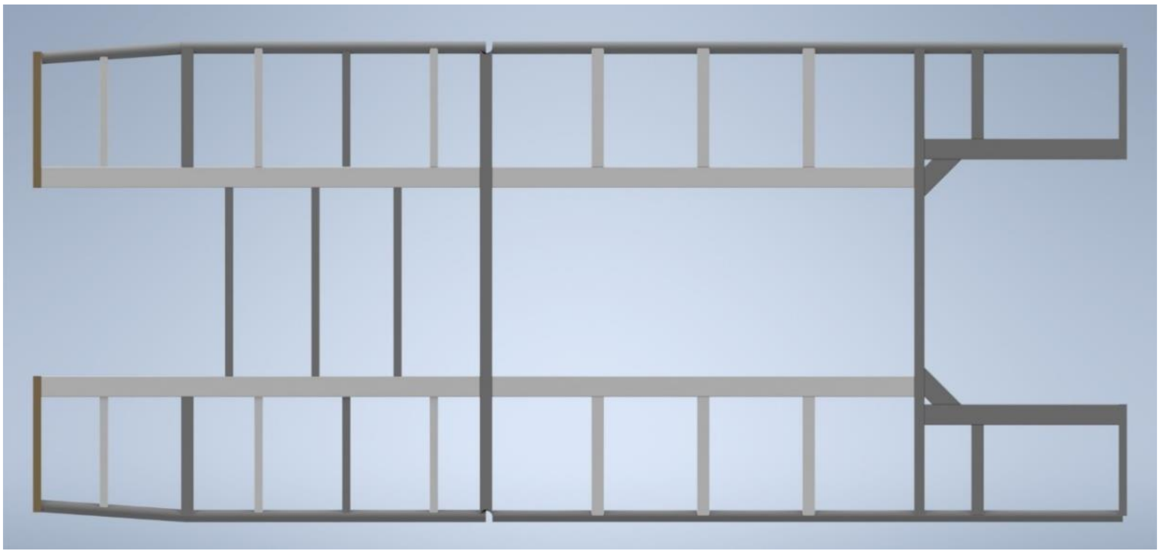

Figure 28. Base plane of the chassis.

Finally, connected to the base plane, 2 firefighting equipment cargo boxes were drawn on each side of the vehicle, as referred during the concept phase of the project, observable in Figure 33.

4.1.2 Cab

It is of cab structure’s responsibility to create a safe space for the occupants. The pod should be capable of withstanding, during any hypothetical accident, extreme loads, while providing an ergonomic, comfortable and operative room, during all missions and commutes.

The cab’s composition begins in the frontal transversal plane, passing on the foremost point of the vehicle, and terminates at the transversal plane that includes the first complete transverse beam of the base plane. The creation of the cabin was executed from the back to the front, since the rear living compartment, where 3 passengers sit, is a more standard part with great similarity to past Jacinto’s projects of cabin extension of OEM trucks. Yet, in this case, and aiming for a tougher, more rigid component, enhancing the overall transversal stiffness of the chassis, integrated roll bars were fitted, 2 vertically and 1 horizontally on the roof. The passenger’s partition can be represented as a 1 400 x 2 080 x 1 500 mm rectangular hollow slot. Besides meeting EN 1846-2 [2], the width and depth enable the fitting of SCBA seats.

The second section of the cabin is the compartment for the driver and front passenger. The design of this part is highly influenced by the fact that it is the element that needs to withstand most of the energy from frontal impacts, as tested by ECE-R29-02 [8] Test A and B; the limited space available for both occupants due to the mid mounted engine, transmission, radiator and other related equipment; and as a consequence of the chosen windscreen and its organic shape. This last element proves to be the hardest to model after, as there was lack of documentation and the existing is unprecise[10]. As a result, a CAD file from Jacinto’s old project portfolio was used, even though, there was no certainty of being the final representation of the actual windscreen. Furthermore, no physical glass example was available to be inspected and measured. Still, to validate the CAD model, and since there was available an old Lusitano cabin used for certification tests, reverse engineering was employed. Measurements were taken to the windscreen support and then compared to the dimensions of digital version. Since the measurements matched, the veracity and accuracy of the available digital version could be verified.

The proposed windscreen has a 1 690 mm lower width and widens to a 1 930 mm upper width. Additionally, from Figure 9 it is possible to understand that the Lusitano’s cab tappers down its breadth towards the front of it. It is, therefore, possible to conclude that the same architectural style is imperative to be employed in Rhino truck. However, for the present under development model this imposes a problem, as the central opening to lodge both engine and transmission does not allow for the front seats to be close together, as observable in Figure 29. As a consequence, a new concern arises. Forward and lateral visibility of the front occupants is reduced, as the A pillar obstructs part of their peripheral view, Still, and since there is no current European standard regulating the outside direct visibility for these vehicles, the top management team decided to proceed and reassess the situation with the full-scale prototype. Another issue caused by the front window is due to the way it widens. Ideally, doors should be straight. Past experiences show that curved ones have the tendency to bend, either due to thermal expansion during operation or due to usage fatigue, result in loss of soundproofing and watertightness of the assembly or even the failure of the closing mechanism. Thus, it is in the

[10] Technical drawing in ANNEX B.

best interest that the door is as straight as possible. To ensure it, a door plane had to be determined, while still respecting the windscreen shape and minimizing the space reduction caused.

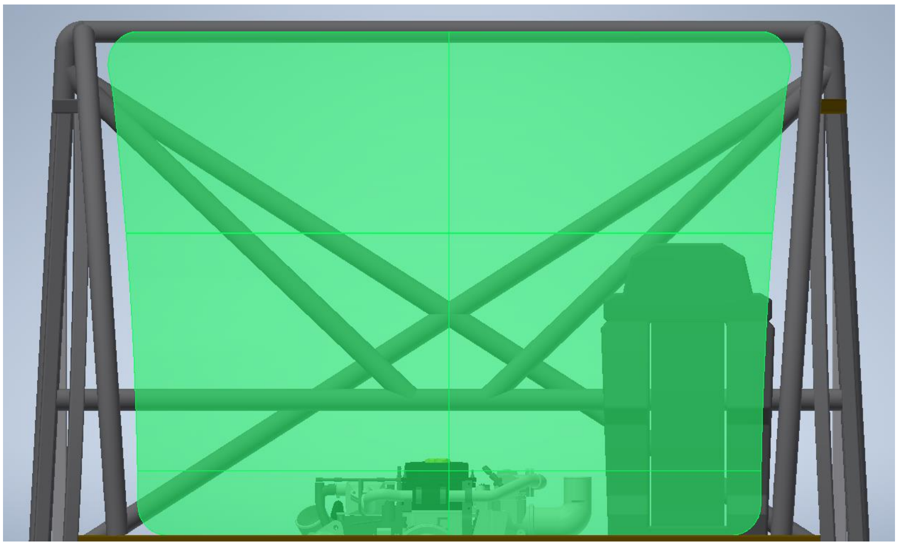

Figure 29. Space limitation in relation to the windscreen.

The final solution, shown in Figure 30, is a narrower front section that widens according to the access plane until the first rollbar, easily understood with the top view of the base plane, in Figure 28. To ensure the tightness and diminish the probability of door bending, a secondary flat beam was drawn next to/below the A pillar, with a similar curvature if laterally looked at the cab. Still, the door hinges will be limited to the lower straight part of the secondary A pillar, meaning that their reliability can only be assured when a prototype is constructed and undergoes long testing.

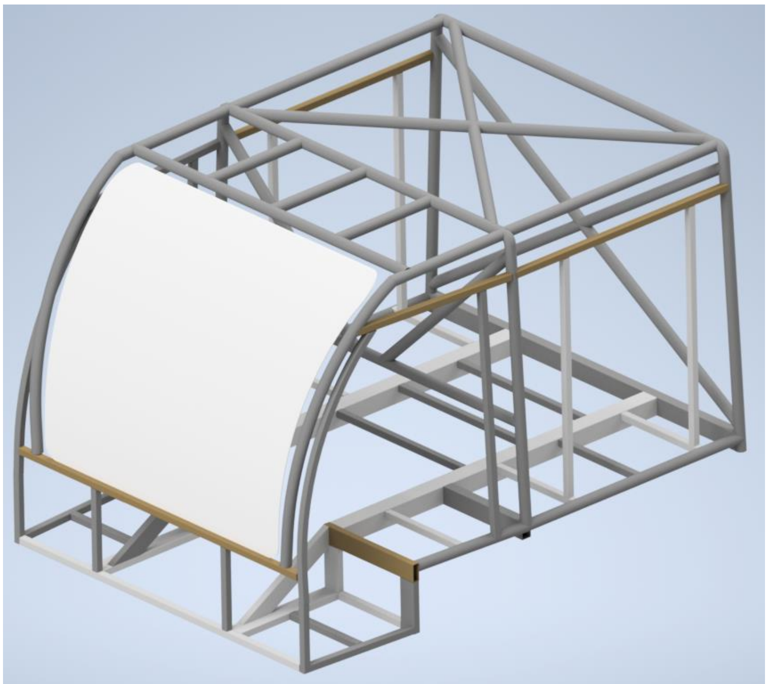

Figure 30. Final iteration of the cabin.

Lastly, it shall be noted that further or different longitudinal stiffening is not possible on the front section, apart from the placed diagonal beam, as space for the radiator and dashboard needs to exist.

4.1.3 Axle support

The axle support is, in the present case, actually, more than just the connection of the chassis to the boogies. It supports the engine, transmission and part of the weight load of the water reservoir, what is more, it is the part of the chassis that endows most of the transversal stiffness of the structure.

The axles are one of the components that will be supplied by an external entity to Jacinto, therefore the link between axles and chassis is completely dependent on the chosen supplier. Thus, the independent suspension axle market was researched and contacts made with possible partners. No agreement nor perfect solution was achieved until the end of the thesis. Nonetheless, from the market research and discussed options with axle producers, most assemblies are constituted by an encased differential and wishbone arm suspension. Furthermore, the mountings to the frame are mechanical fastened connections based, as shown in Figure 31.

Figure 31. ADS AX75 Independent Axle [50].

Since no final solution was obtained, a flat rectangular 1 000 x 800 mm connecting section was assumed. This segment will be bolted to the beams in red of Figure 32. Lastly, truss derived construct was used for a greater vertical distribution of loads.

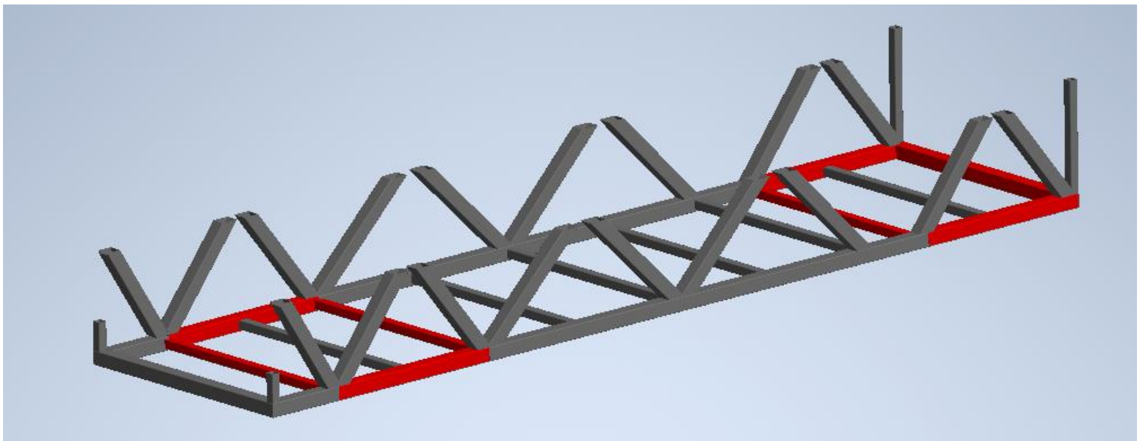

Figure 32. Final iteration of the axle support.

4.2 Obtained chassis

One last iteration of the chassis was obtained around 2.5 months after the beginning of design process, as no further fruitful developments with equipment suppliers were occuring. Thus, assuming that no solution for the axles was still achieved with the list of providers in dialogue with Jacinto and that the impact of the position of the A pillars on driver’s visibility could only be assessed with a real size prototype.

Additioanlly, it should be noted that even though the final render of the strucute, Figure 33, includes an axle configuration provided by Timoney, an Irish supplier, it is only for demonstration purposes. As it does not meet the desired width of the vehicle, being too wide, nor fit the current layout of the chassis' axle support.

Figure 33. Final chassis.

In final note, all the used beam sections can be found in ANNEX C.

4.3 Chassis validation – FEM simulations

To verify the structural integrity of the chassis developed 5 FEM simulations, using SIMULIA Abaqus 2020 software, were modelled and computed: 1 static with the expected weights the structure will face in normal operational running order, another static situation simulating a transposition of an obstacle and 3 dynamic ones regarding the cab's safety in case of accident.

4.3.1 Model, material and mesh

For the FEM study of the chassis and for simplification purposes, the structure was remodelled directly in the SIMULIA Abaqus 2020 software as a wired part. By way of explanation, it was drawn a skeleton, representing the middle axis of all profiles. Instead of opting for solid parts, wire part was chosen with the aim to reduce the demand of computational performance, reducing the time of calculations and the memory required, while achieving representative and accurate result, nonetheless. Subsequently, the respective sections will be assigned to the wired frame.

Lastly, and since all structural profiles composing the chassis are made of an S275 steel, the material properties have been obtained from EN 1993-1-1 Eurocode 3 [51] and checked in Fei Yang and Milan Veljkovic paper [52]. The values are presented in Table 7, and were introduced into the FEM program.

Table 7. Material properties for S275 steel [52]

Material properties	S275 graded steel
Density, ρ (kg/m^3)	7 850
Young's modulus, E (MPa)	210 000
Poisson's ratio in elastic range, ν	0.30
Yield strength, f_y (MPa)	275
Tensile strength, f_u (MPa)	430
Strain at yield strength, ε_y (%)	0.158
Strain at tensile strength, ε_u (%)	22

Since the dynamic studies conducted, following ECE-R29-02 [8], focus on the deformation that certain impacts and crushing loads cause to the cabin, the nonlinear behaviour of the material is also necessary. To obtain these values an expedite method, derived from the aeronautical industry, was used, the Ramberg–Osgood model [53, 54, 55, 56]. The engineering stress-strain curves of a material are plotted, using the model, assuming an exponential relationship between stress, σ, and plastic strain, ε_p, equation 4.1.

$$\varepsilon_p = 0.002\left(\frac{\sigma}{f_y}\right)^n \tag{4.1}$$

Where:

- σ is stress;
- f_y is the yield stress;
- ε_p is the plastic strain;
- n is the Romberg-Osgood parameter.

Developing 4.1, and since the total strain, ε, is the sum of the elastic plus the plastic strain, comes equation 4.2:

$$\varepsilon = \frac{\sigma}{E} + 0.002\left(\frac{\sigma}{F_{ty}}\right)^n \tag{4.2}$$

Where E is the Young's modulus and n is obtained by equation 4.3.

$$n = \frac{\ln\left(\frac{100 * \left(\varepsilon_u - \frac{f_u}{E}\right)}{0.2}\right)}{\ln\left(\frac{f_u}{f_y}\right)} \tag{4.3}$$

Finally, it is possible to plot the true stress-strain curve by transforming the stress and strain values to their true magnitude, accounting with the reduction of area while under tension during the properties assessment test, resorting to equations 4.4 and 4.5.

$$\sigma_{true} = \sigma * (1 + \varepsilon) \tag{4.4}$$

$$\varepsilon_{true} = \ln(1 + \varepsilon) \tag{4.5}$$

Figure 34presents both the engineering and the true stress-strain curves. Noticeably, it is the true plastic values that are introduced in the numerical analysis software and are listed in ANNEX D.

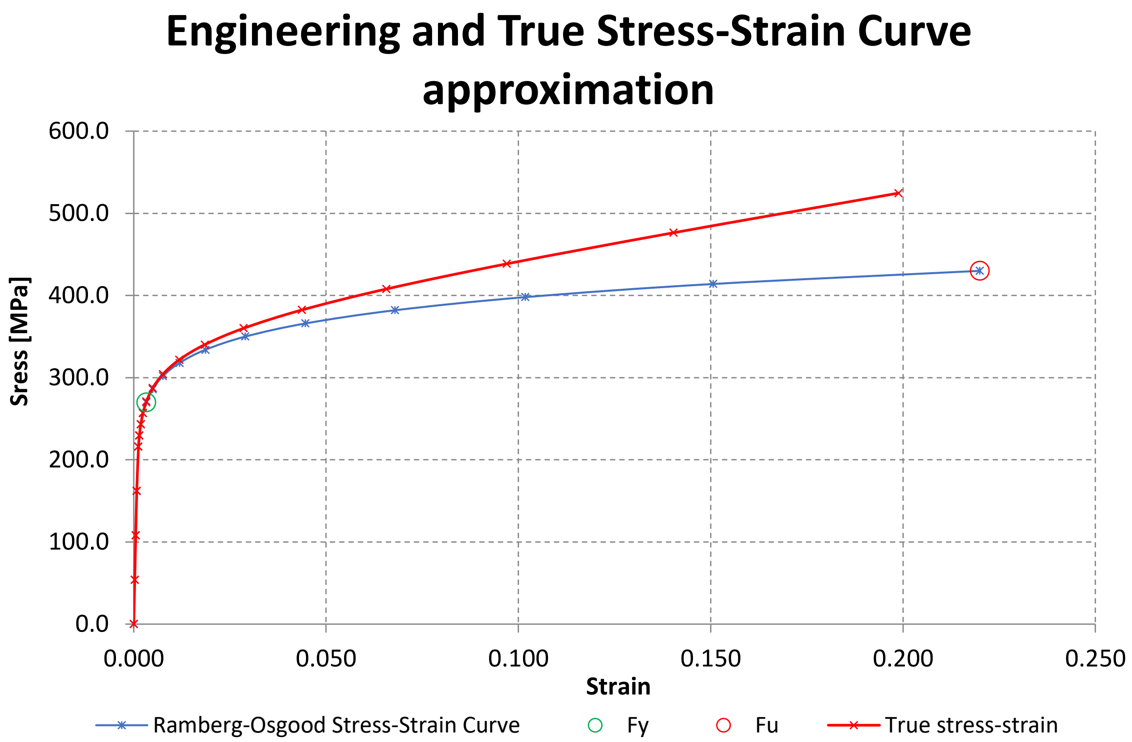

Figure 34. Engineering and True Stress-Strain Curve approximation using Ramberg-Osgood model – S275.

One last crucial factor to all numerical analysis is the mesh. Since the structure was drawn as a wired part, 1 dimensional element, the refinement of the mesh is limited only to the size of the elements of the mesh. To achieve an adequate seed dimension a convergency study was carried. The study was conducted using the first case of the static scenario presented in the next section 4.3.2 and it is available in ANNEX E. The final mesh has a 1.5 mm seed size and is composed by 121186 elements Furthermore, the element type of the mesh was set to standard linear beam element, B31.

4.3.2 Static load scenarios

The first FEM simulation has the aim to confirm the chassis' capacity to withstand the normal weight loads associated with the water tank, crew and all equipment that will be equipped and carried on the vehicle. In other words, along with the permanent mobile components already presented in Table 2, other element weights will be considered, such as seats and occupants, hoses and nozzles and sapper firefighting equipment. The mass of these equipment, that add up for the gross laden mass of the vehicle, GLM, are presented in Table 8. The occupants' mass is also considered in the GLM and is standardized by the second part of the norm EN 1846 [2]: the driver weights 75 kg plus its equipment sum another 15 kg[11], while the rest of the crew stacks up to 90 kg each.

[11] Considered as one in the simulations, driver's mass equivalent to 90 kg.

Table 8. Equipment carried by the truck

Equipment	Mass (kg)
SCBA seat[12]	25
Hoses and nozzles	500
Sapper firefighting equipment	700
Backup petrol water pump	30

The mass loads will be applied as 8 independent groups in each respective CG relative to their position in the frame: front occupants; back occupants; engine and transmission; water tank; sapper firefighting equipment; water pump; backup pump; and hoses and nozzles. The sapper equipment was considered to be stored on the front boxes, while nozzles and hoses transported in the back ones. The distribution of the resultant forces is presented in Figure 35.

Along with the definition of the loads, the characterisation of the boundary conditions is crucial for the achievement of representative results. In this case, in a real scenario, the limits of the vehicle are the points of contact of the truck with the ground. Since only the chassis is under study, the boundary conditions admitted are the axles. The points of contact between the axle assembly and the structure, as confirmed by Figure 31, are the differential carrying block and the suspension spring/damper. The red central longitudinal beams will be considered to have no degrees of freedom, displacements and rotations locked, while the suspension point will be considered as a single support in the vertical direction. As this is a static study, the damping of the suspension can be ignored and the single support will only be dependent on the elastic element. Since the choice of axles is still not confirmed, the spring of the suspension is also not known. Therefore, to obtain an adequate spring stiffness, the coil of the axle assembly provided by Timoney, and represented in Figure 33, will be used as the reference. Through equation 4.7, the development of equation 4.6, the spring rate, k, can be obtained [57, 58].

$$k = \frac{F}{y}$$

$$F = \frac{G\, d^4\, y}{8\, D^3\, n} \tag{4.6}$$

$$y = \frac{8\, D^3\, n\, F}{G\, d^4}$$

Where:

F	is the spring force;
y	is the deflection of the spring;
G	is the modulus of rigidity of the spring material;
d	is the nominal diameter of wire of the coil;
D	is the diameter of the coil;
n	is the number of active coils, coils that suffer deflection.

[12] The driver's seat, even though not a SBCA ready will be considered to weight the same.

$$k = \frac{G\, d^4}{8\, D^3\, n} \tag{4.7}$$

Additionally, and not knowing the exact material of the coil, resorting to EN 13906-1 [58] and considering the diameter, *d*, of the coil, the modulus of rigidity, *G*, can be found. Table 9 provides the necessary properties of the spring to calculate *k*.

Table 9. Timoney spring properties

Property	**Units**	**Magnitude**
G [58]	N/mm^2	78 500
d	mm	43.200
D	mm	202.915
n		7

The spring rate, *k*, is equal to 584.351 N/mm. And it will be assigned to the middle point of the beams coincident to the centre transversal plane of the axis, as demonstrated by the pink globes in Figure 35.

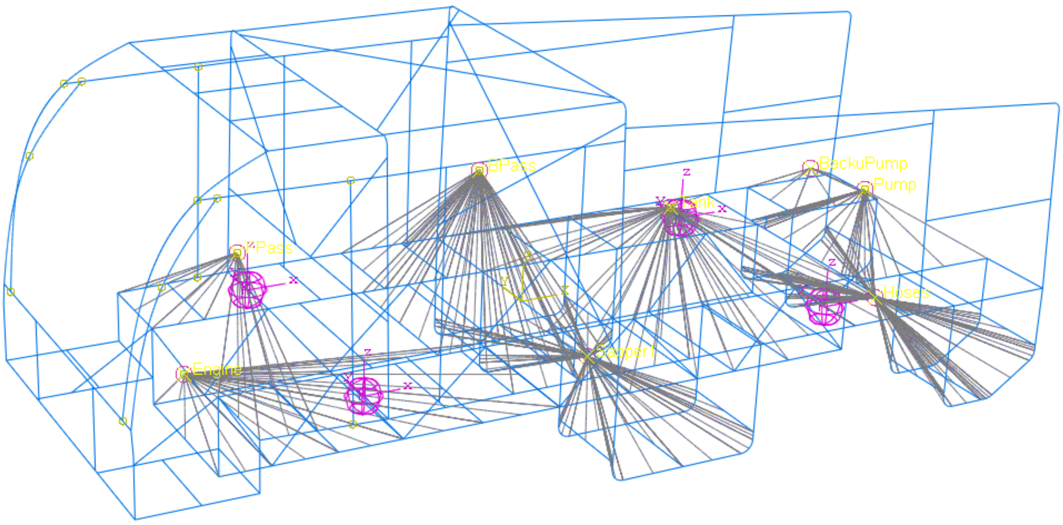

Figure 35. Load distributions and spring locations.

Lastly, a safety factor should be applied in the calculus. In this case it was considered a safety factor, SF, equal to 3 and calculated through equation 4.8.

$$SF = \prod^{i} SF_i = SF_{dynamic} * SF_{standard} \tag{4.8}$$

Where the standard safety factor, $SF_{standard}$, of 1.5 is multiplied by a dynamic safety factor, $SF_{dynamic}$, equal to 2, to ensure that the structure not only is capable of withstand the masses while the acceleration is zero, stopped or with constant speed and no disturbances, but also when breaking, accelerating, or facing small obstacles, such as holes or bumps. To summarize, all loads will be multiplied by three, to achieve conservative results.

After calculation, the simulation, presented in Figure 36, demonstrates that the structure integrity is under threat for the normal operational conditions that the vehicle will face. As the maximum stress obtained, 302.4 MPa, is already in the plastic regime of the material, which is higher than the yield strength of 275 MPa. Furthermore, it can be said that the maximum stress point is found in the axle support, in a small portion of the component that does have a discontinuity of the truss architecture and that could only be reinforced with a vertical beam. Moreover, the influence of the value of the safety factor used can not be disregarded and 3 can be considered as a very conservative parameter. Thus, if the $SF_{standard}$ is neglected and the used SF is limited just to the $SF_{dynamic}$, the obtained max tension will decrease by 1.5 times, resulting in a 201.9 MPa. This magnitude is below the plastic regime entry threshold, therefore ensuring a safe loading condition during regular operative.

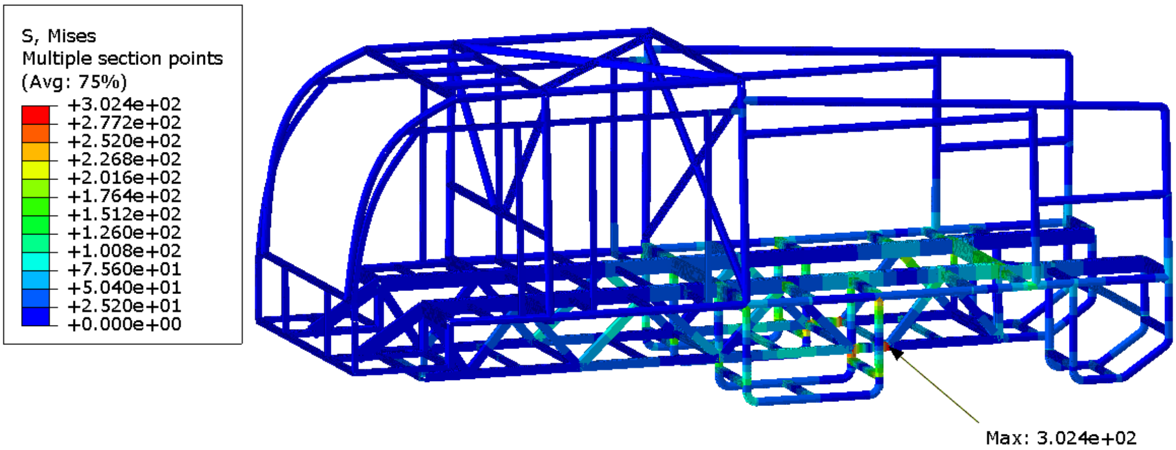

Figure 36. von Mises Stress - static simulation.

A second static simulation is performed to simulate a compression caused by an obstacle on the road, like a rock or log. To achieve, along with the spring rate, already estimated, also the stroke of the suspension shall be known. The positive suspension travel, based on the ADS model [59] presented in Figure 31, was admitted to be 180 mm. A bump height of 120 mm was considered and subjected only to the front left suspension, the driver side, by the means of a displacement on the base of the spring. Besides, all weight loads are not multiplied by any SF and are applied with their true magnitude.

From the asymmetrical simulation the following results are obtained, Figure 37. The maximum von Mises stress is of 294.6 MPa, above the yield stress, and is found in the beam where the spring actuates. The value should be taken with a pinch of salt, since the spring rate was determined using reverse engineering and because the spring force is acting in a single point, which is not totally representative of how the load is transmitted to the structure. Another aspect to take into account is the fact that the structure has no freedom of movement due to the central connection. In a real scenario, the axles will allow for the chassis to rotate. This rotation would lead to a more evenly distribution of the force to the rest of the suspension elements. Nevertheless, this can indicate the need for reinforcement in the area, employing more beams or bigger and different sections.

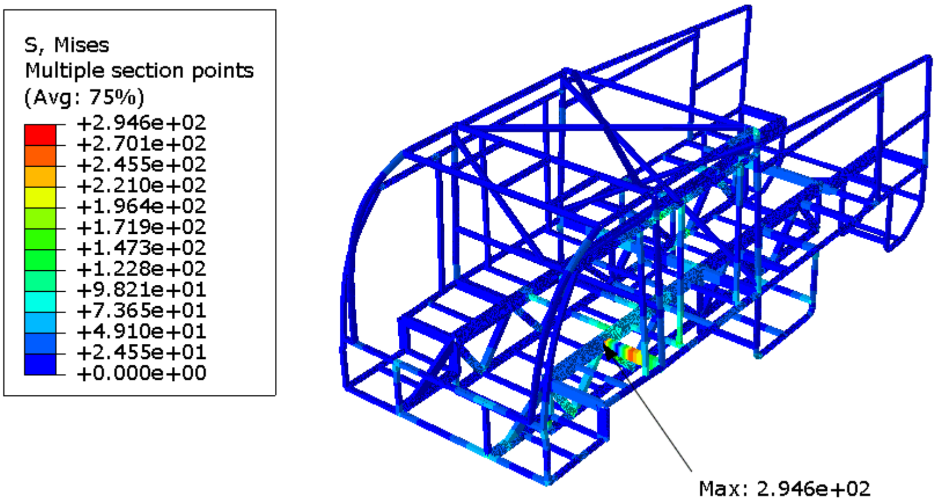

Figure 37. von Mises Stress - static bump simulation.

4.3.3 Test A

As explained in 3.2.2, the tests to certify a cab, according to ECE-R29-02 [8], can be performed using numerical methods instead of full-scale physical assessments. It is within this scope and respecting the test requirements that the following FEM simulations were modelled.

As exposed previously, to simulate a front impact, a flat rectangular 1 500 kg impactor will be freely dropped on a rotational apparatus, hitting parallelly the cabin in the foremost point of it. Since the described trajectory of the block is circular, to simplify the modelling of the simulation it is possible to consider a linear movement at a velocity equal to the tangential speed of the impactor at the contact point.

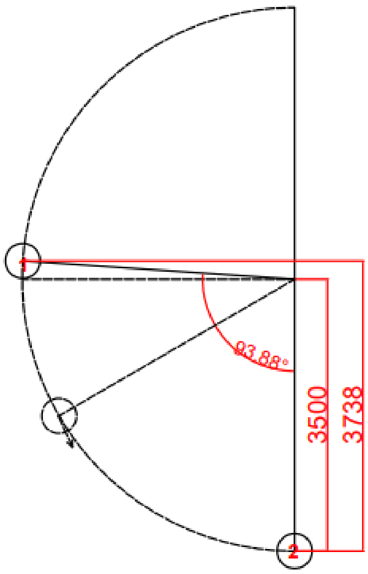

Figure 38. Schematic of Test A.

An expedite approach for this determination is by resorting to the Conservation of Energy Principle, that states that the initial energy of the system is equal to the final energy of it, as in equation 4.9, representing *1* and *2*, initial and final states, *K* and *P*, kinetic and potential, *m*, mass of the pendulum, g[13], the acceleration of gravity, and h, the height of the vertical distance from the pendulum to the striking point, respectively.

$$\begin{gathered} E_1 = E_2 \\ E_{K_1} + E_{P_1} = E_{K_2} + E_{P_2} \\ \frac{1}{2}mv_1{}^2 + mgh_1 = \frac{1}{2}mv_2{}^2 + mgh_2 \end{gathered} \tag{4.9}$$

Furthermore, the regulation [8] also requires that the impact energy shall be of 55 kJ. This energy is characterized by only having the kinematic part. Assuming that all the kinetic energy is transmitted from the block to the structure, through equation 4.10, it can be concluded that the impactor needs to be travelling at a linear velocity of 8563.49 mm/s.

$$55\ kJ = \frac{1}{2}mv_2{}^2 + 0 \tag{4.10}$$

It can also be stated that the two holding beams, in the case of a physical test, shall have a length, L, of 3 738 mm to be released at a 90° angle or for the standard minimum 3 500 mm span, using, trigonometry based, equation 4.11, the pendulum should be angled at 93.88°, as represented in Figure 38.

$$\alpha = 90 + \sin^{-1}\frac{\frac{55\ \text{kJ}}{g * m} - 3500}{3500} \tag{4.11}$$

After the speed of impact is calculated and the impactor modelled as a rigid body with a mass of 1 500 kg, it is possible to configure the rest of the simulation parameters. The impactor was positioned 10 mm from the foremost plane of the chassis and the initial speed was set. The contact will run on an explicit dynamic step and was defined as a general contact. The contact behaviour was characterized as frictionless tangentially and in the normal direction as hard contact and allowing separation after interaction. Finally, the mesh was reworked to enhance the results obtained from the simulation. This is to say, that the overall mesh had its seed size increased to 2 mm, thus the number of elements reduced, while the beams contained on the frontal plane had the seed size decreased to 0.5 mm, in order have a better refinement in the contact region. Globally the number of elements of the chassis' mesh is of 107 872 elements. In the case of the impactor, the type of element is defined as quad structured and the seed size is set to 5mm, resulting in 80 000 elements.

At the start of the simulation, it was possible to check that the kinetic energy was equivalent to the regulated [8] 55 kJ. The simulation was forced to terminate after 32 133.7 s (≈ 9 hours) of CPU time and representing a total simulation time of 0.068 s. This decision was based on two assumptions. The first one is based on the time needed for the pendulum to strike the structure, the first contact occurs at $1.168*10^{-3}$ s. And the second conjecture is founded up on the evolution of the kinetic energy has over time, when the zero is reached, no movement exists on the system, thus all energy was transferred. This is to say, that in the current case, the condition of contact is verified, time superior to $1.168*10^{-3}$ s, and the kinect energy has already inverted its trend, i.e., has already started to increase back again after reaching a low of less than 200 J, as shown in ANNEX F.

The recorded maximum von Mises stress, as seen in Figure 39, is found on the central diagonal beams near the base of the driver and front passenger seats. Moreover, the significant

[13] g=9.81 m/s^s was used.

resulting stresses are confined to the cab partition of the chassis. It can also be stated that it is equivalent to the last value computed for the true stress-strain curve, Figure 34, thus the limit for further calculation is reached and the failure of the material is imminent.

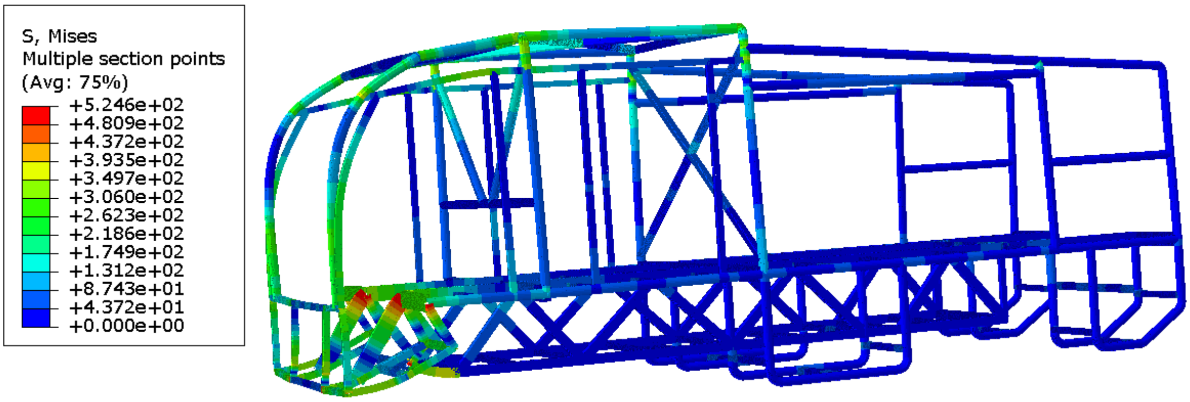

Figure 39. von Mises Stress - Test A simulation.

When the stresses on the direction of impact are analysed, S_{11}, in Figure 40, the same conclusions, on the same locations, can be drawn, along with the type of loading each beam is subjected to, either traction or compression. Noticeably, the front feet platform is subjected to high compression while the frontal part of the base plane of the chassis is subjected to tractive forces with similar magnitude.

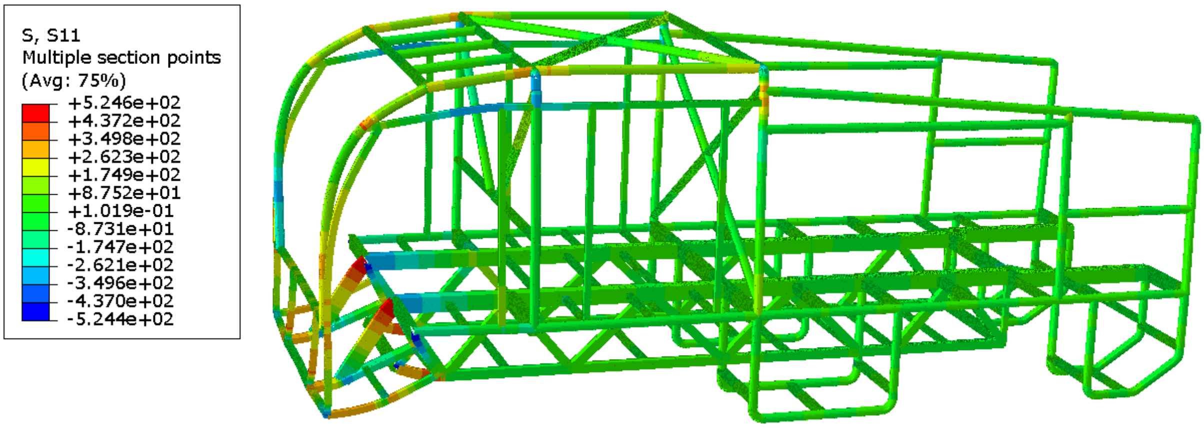

Figure 40. Longitudinal Stress - Test A simulation.

Finally, the most relevant data to certify the cab under ECE-R29-02 [8] is the presence of big displacements of beams and if there is the possibility of contact with the occupants. In this case, as observable in Figure 41, the maximum overall displacement is obtained on the frontal plane beams, with a down movement towards the interior of the cabin, reaching an utmost value of 301.9 mm. The transversal displacement, U_{22}, is ignorable as it will never pose a threat to the occupants. The vertical displacement, U_{33}, can also be disregarded as despite its greater magnitudes to 20 mm it does not create big dimensional differences, the translations are equivalent in each vertical axis. Yet the impact direction, i.e. longitudinal to the chassis, is, ultimately, the critical direction of the deformation, since it is the direction of the occupants, being represented in Figure 42.

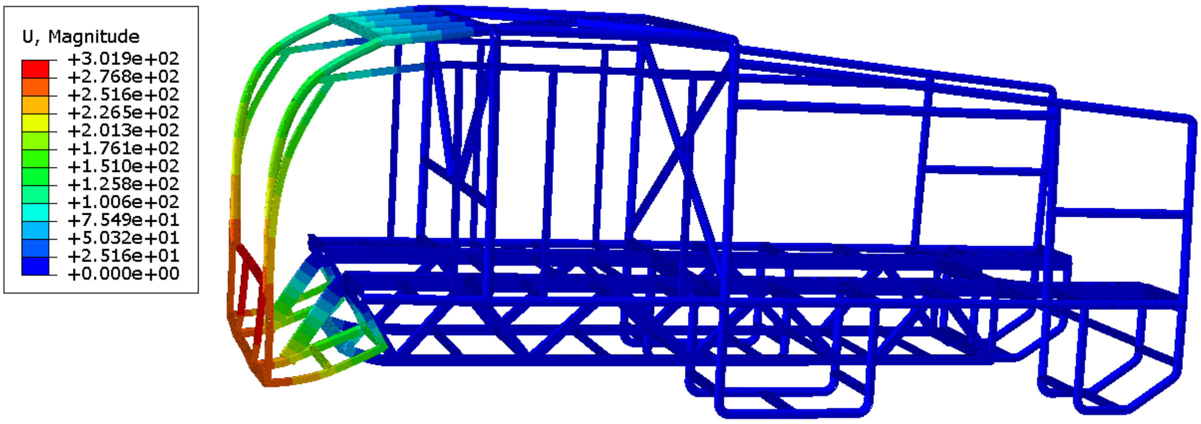

Figure 41. Maximum displacement - Test A simulation.

The maximum U_{11} displacement occurs at seat height and the deformation has a magnitude of 222.5 mm. Therefore, it is at the height of occupants' knee, that the possibility of collision should be assessed. Since the final configuration and arrangement of the cab's interior is still to be defined, it is not possible to confidently confirm if the cab is certifiable or not. However, with an opposing line of thought, the maximum depth of the dashboard can be deducted, ensuring that it does not hit the occupants in case of a front accident. The available space, on an undeformed structure, between the seat and the front plane is of 650 mm, this value is reduced to 350 mm when subtracting the minimum 300 mm, standard [2] imposed, required span for the legs and feet. So, accounting with the max deformation, the dashboard's depth is limited to an impracticable 127.5 mm.

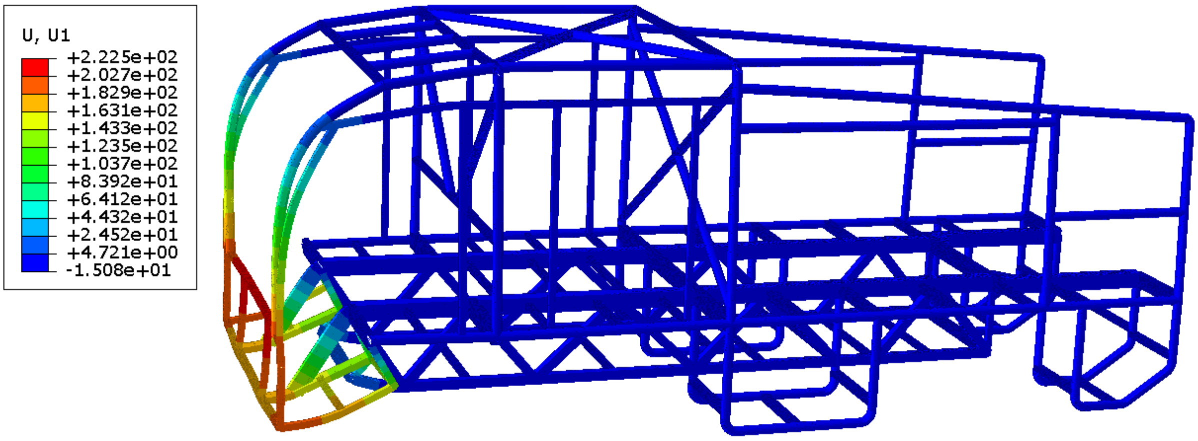

Figure 42. Longitudinal displacement - Test A simulation.

It should be noted that, since there is no final position for the engine, transmission, nor configuration for the steering system, these components are not considered during the simulations. Other regularly fitted structural element on these vehicles are external ROPS[14]. Thus, same rigidity and mechanical capacity to withstand impact loads is not present. Nevertheless, a reinforcing beam mirrored to the most stressed beam and an increase in size or thickness of the vertical most bended beams would greatly enhance the behaviour of the cab under frontal impact, reducing the deformation and the maximum stress observed.

[14] Roll Over Protective Structure.

As a final remark and even though the current front longitudinal stiffening elements are unable to limit the deformation of the cabin, the bending that the frontal part of the cabin suffers on the lower section can be considered beneficial as it moves away from the vital space. Accordingly, if the rotation would take place even further the better. This can be achieved with the addition of the just recommend beam.

4.3.4 Test B

With a homologous line of thought to the previous test, 4.3.3, the 1 000 kg cylindrical impactor shall be carrying a linear velocity of 7 668.12 mm/s to reach the regulated 29.4 kJ impact energy. If considered as a perfect system with conservation of the energy, in a real scenario, the pendulum should be elevated 2 997 mm from the striking point. Since ECE-R29-02 [8] regulates that the holding members have at least 3 500 mm and resorting to the trigonometry, by equation 4.12, it means that a minimum sized apparatus should have its cylindrical mass angled to 81.74°, as in Figure 43.

$$\alpha = 90 - \sin^{-1}\frac{3500 - \frac{29.4\ kJ}{g * m}}{3500} \qquad 4.12$$

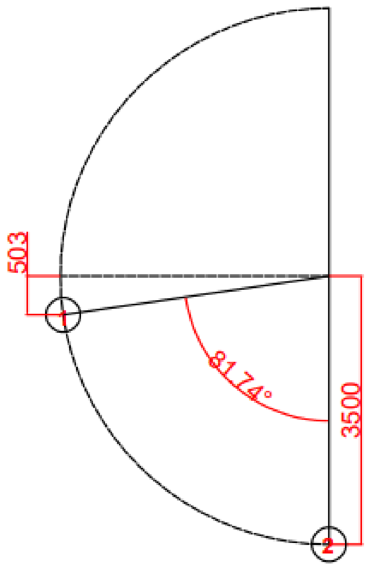

Figure 43. Schematic of Test B.

The assembly of the simulation is carried similarly to the previous one, Test A (section 4.3.3), with the exception of the meshing. The impactor mesh seed size is set to 7 mm in the contact side with quad structured elements and 20 mm in the inactive faces resorting to a free mesh technique, overall, the rigid body counts with a total of 64 974 elements. Furthermore, the chassis' mesh was partitioned in 3: back section, the tank and storage area, with a seed size of 5 mm, overall cab beams with 2 mm and A pillars and surrounding beams 0.5 mm. In total 90 985 elements are generated to simulate the chassis behaviour.

Likewise, the initial kinetic energy can be confirmed to be of 27.4 kJ, as governed by ECE-R29-02 [8] and the identical simulation stop criteria is again employed. In this case, the job was terminated at 23 584.3 s (≈6.5 hours) of CPU time, representing 0.130 s of simulation, as shown in ANNEX G.

The first results to analyse are the stresses and their distribution, followed by the displacements occurred. Figure 44 presents the computed von Mises stresses. Remarkably, the highest value, substantially inferior to the material's 430 MPa tensile strength, is reached on the lower section of the front plane and not on the A pillars where the impact happens.

Additionally, in contrast to the structure geometry and load scenario, the distribution of the stresses is found to be not symmetrical.

The max stress location can be explained either due to problems during the definition of the geometry, mesh or boundary conditions; or because of any abusive approximation that the software may have made during the iterative process of the stress calculation. Since no errors were found on the model nor boundary conditions, it can be admitted that the issue shall be related to the computing process or mesh imperfections, ultimately the computing of the contact between impactor and structure. Besides, this first premise may explain the second, the asymmetry in the distribution of stresses. The rerunning of the simulation resulted in similar results.

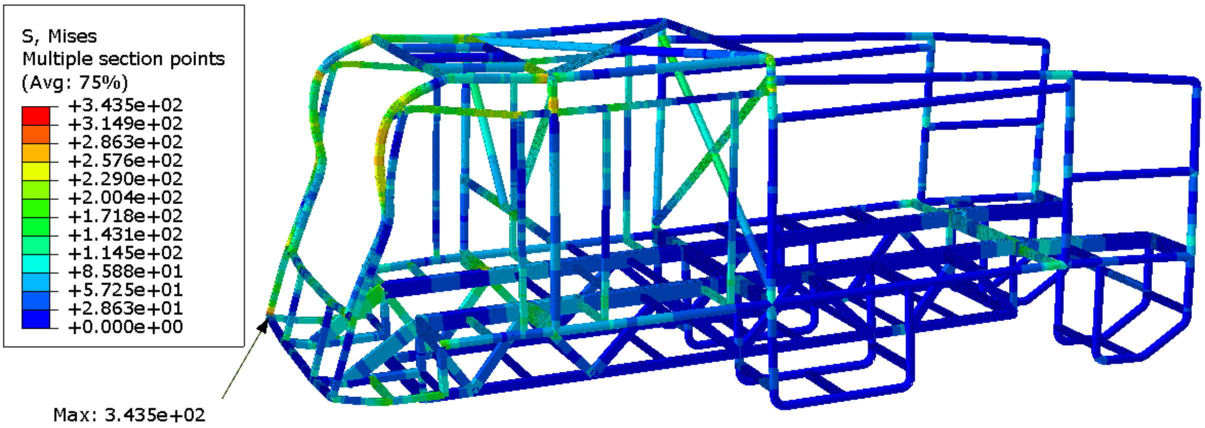

Figure 44. von Mises Stress - Test B simulation.

When it comes to the displacements, the same premises as for Test A, in section 4.3.3, can be employed, i.e. U_{22} and U_{33} are neglected. The longitudinal displacement, U_{11}, is, again, the critical one, presenting a maximum value of 351.4 mm. Even so, and thanks to the curvature of the windscreen, this value is not worrisome and is not enough to put into stake the certification of the cab.

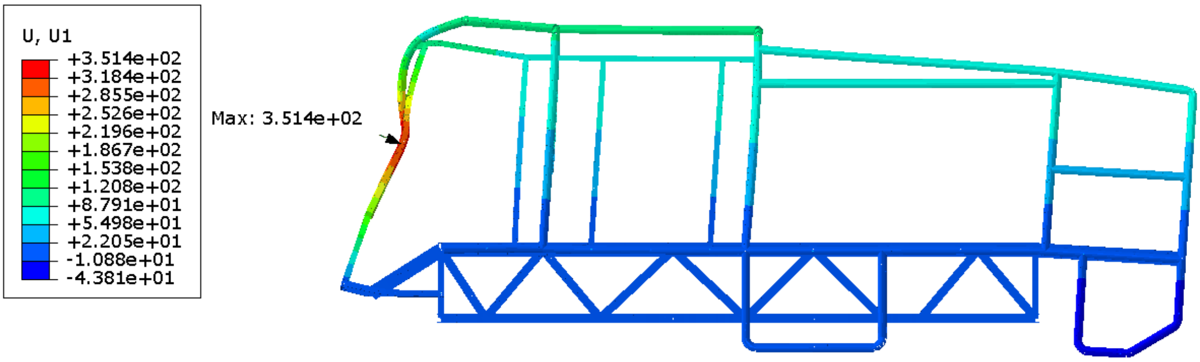

Figure 45. Longitudinal displacement - Test B simulation.

Lastly, it is possible to state that the overall bending suffered by the chassis is also not dangerous to occupants. Hence, the structure passes the Test B, even without the required equipment.

4.3.5 Test C

The last test is characterized by two consecutive loading scenarios. The first one, P_1, is an impact case and it is followed by a secondary, P_2, crushing state.

When it comes to the first condition, P_1, the regulation [8] implies that the energy generated by the impact of the flat impactor to be of 17.6 kJ. As carried in 4.3.3, it is possible to compute, by equation 4.10, the linear speed that the pendulum will hit the structure. The mass will strike perpendicularly at a linear velocity of 4 844.24 mm/s. Furthermore, this speed can be decomposed in vertical and horizontal direction, as in Figure 46, and their magnitude is of 4 552.10 mm/s in the horizontal direction, *x* in the figure, and 1 656.83 mm/s in the vertical direction, *y*.

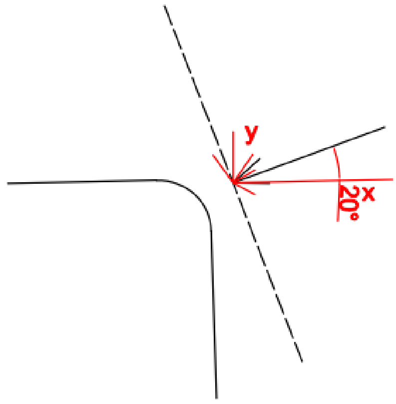

Figure 46. P_1 speed decomposition.

The second loading instant, P_2, is a crushing condition, applied by a press. It will be equated using a distributed force applied on the top beams that make up the roof of the cab. The magnitude of the force, since the axles are to be chosen, will be considered as the maximum regulated [8], 98 kN.

The pendulum's mesh was defined as a single element, quad structured and the chassis mesh as two portions. The overall seed size is set to 2 mm and in the wires that will have loads applied set to 0.5 mm, the resulting number of elements is of 92 380. Furthermore, the explicit dynamic job was configured with 3 distinct steps. The first one is responsible for the preload condition, P_1, and totalizes 0.08s of simulation. The intermediate moment has the goal to pull back the impactor, to make sure that it is not influencing the structure during the last phase. The pendulum retracts horizontally during 0.12 s. The final step represents the compressive state, P_2, and lasts for 0.10 s.

As previously, the initial kinetic energy of the simulation was checked and the speed confirmed to be well determined. When analysing the results, it can be identified that the greatest von Mises stress value is achieved during the preloading step and reaches 407.8 MPa, as shown in Figure 47. This value is a safe value, below the tensile limit and is positioned on a bottom section of the chassis.

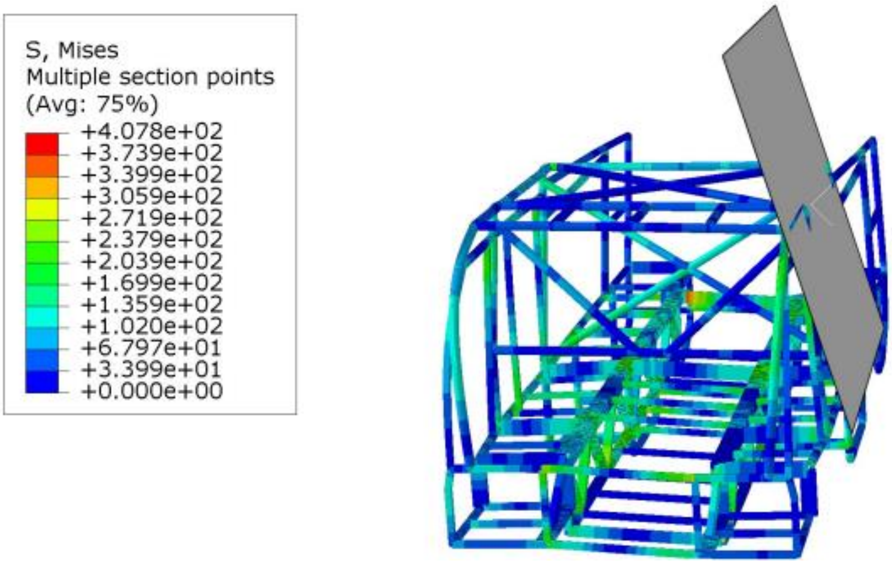

Figure 47. von Mises stresses - Test C simulation- P1.

As a result of the pressing force, the maximum von Mises stress value is of 348.3 MPa. By Figure 48, it is evident that the highest values are distributed along the roof beams.

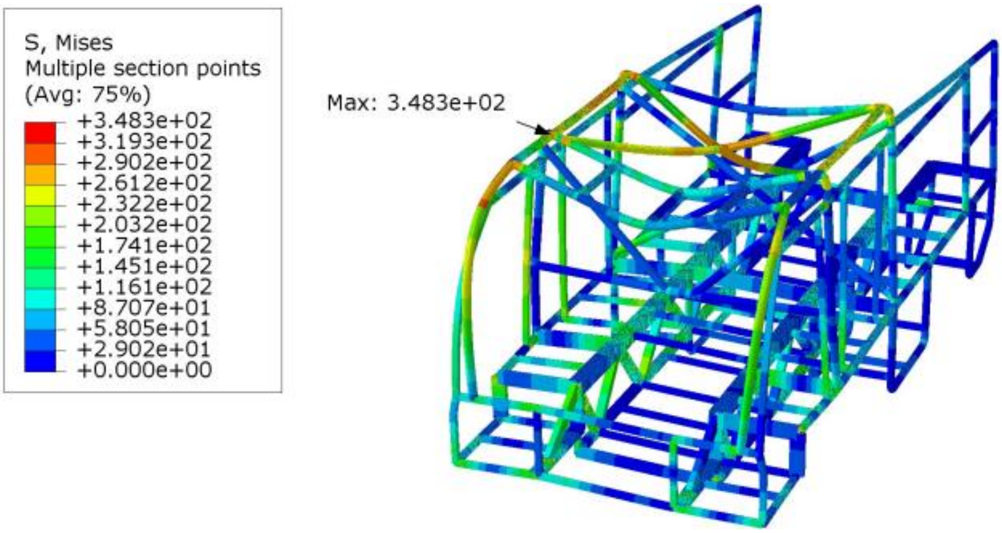

Figure 48. von Mises stresses - Test C simulation- P2.

When it comes to the deformation caused by the impact, it is more meaningful laterally rather than vertically, doing justice to the strike angle. The 164.3 mm transversal displacement occurs in the top section of the cab, as observable in Figure 49, while the vertical is of less than 55 mm on the collision side wall.

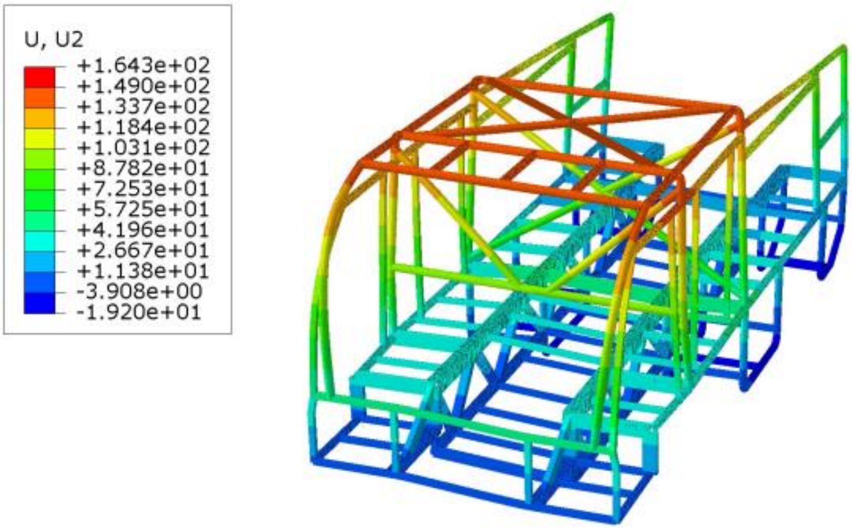

Figure 49. Transversal displacement - Test C simulation- P2.

The most critical movements of the chassis appear during the 180° rollover, the compression step, where the vertical displacement is maximum for the front part of the roof, reaching a value of 316.2 mm. By analysing Figure 50, it can be stated that, even though of high magnitude, due to the V-shape of the deformation, the beams may not enter in contact with the occupants. Yet, this statement can only be verified whenever the complete interior disposition with the seats is decided. Still, it should be safer to increase the cabin height by 250 mm along with a reconfiguration of the front rollbar to further increase the vertical rigidity in the centre of the frame.

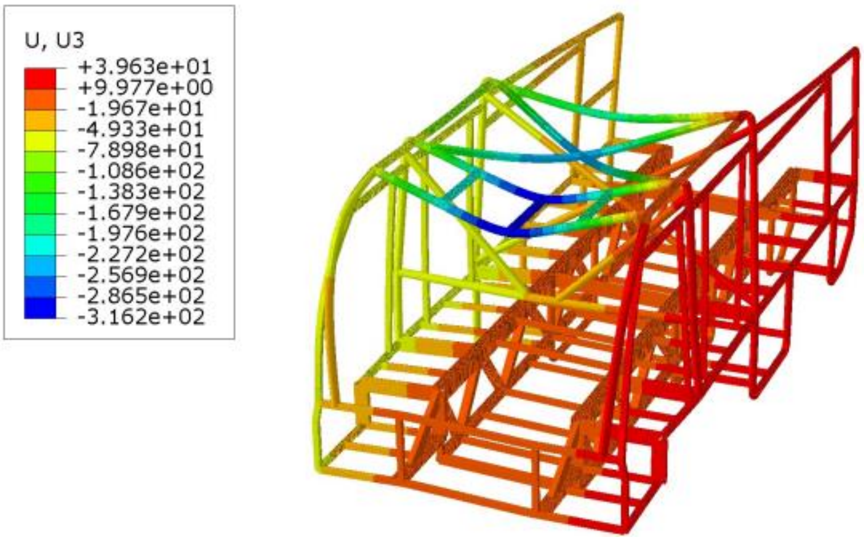

Figure 50. Vertical displacement - Test C simulation- P2.

In final note, similarly to what was mentioned at the end of the two other dynamic tests analysis, the lack of components reduces the real capacity of the strucutre. Thus, with the placement of the doors and the windscreen, the displacements of the roof shall be reduced.

5 Conclusions and future works

5.1 Concluding remarks

It was with the aim to develop a groundbreaking solution for the forest firefighting vehicle market, that Jacinto's top management team has envisioned a truck concept. The project consisted of the creation of a product that can be primarily manufactured and assembled in-house. To unsure the uniqueness and differentiative argument, an initial market research was conducted and planned requisites compared. Parallelly, applicable norms and regulations were searched, emerging EN 1846 [1, 2, 3] and ECE-R29-02 [8], and their implications studied. Overall, it was found that the established requirements meet the identified standards and if respected can generate a far more capable machine, then the available ones on the market.

The initial practical phase was the sketching of the chassis structure. This stage could be characterised as an iterative process with frequent presentations and discussion between all parties involved in the project. It was divided into 3 big moments corresponding to 3 distinct parts, base plane, cab and axle support. The design followed a sequence from the part with more past experience in the company to the least expertise and least information. The base plane was drawn with a heavy influence from other Jacinto's models and with the addition of central core stringers. Next, the cabin was sketched. This element proved to be most demanding to model because of the prechosen windscreen, the allocation of space for engine and transmission and due to the applicable standards having strict dimensions for the occupant's living space that need to be met. Lastly, to create the axle support there was the need to assume an axle width, that corresponded to the breadth of the water tank, as there was no final axle chosen. The component was also opted to be vertically derived from a truss architecture. The final assembly ended up being 100 mm wider than the initial concept, to ensure a lower CG and more space of crew and equipment.

The following phase was the validation of the chassis integrity through 2 different static load conditions and subsequent simulation of the testing required by ECE-R29-02 [8] standard, resorting to FEM software. The first step was to model the chassis as a wired part in the Abaqus software, followed by the gathering of the material properties and calculation of its plastic regime, using Ramberg-Osgood method and finalizing with a mesh convergence study to guarantee a correct mesh size.

The first scenario that was studied was a static loading condition, where all equipment and crew weights are applied and reproduces both stationary and rolling state of the truck. Therefore, a safety factor equal to 3 was initially conservatively considered, yet, and since this would lead to the overpass of the plastic threshold, was at the end considered as 2. This lower SF is admissible for the dynamic representation intended and the maximum obtained values are part of the elastic regime, thus verifying the capacity of the structure to withstand the normal solicitations resultant from fire combat missions.

The second static load state aimed to represent an asymmetrical ground contact, for instance the transposition of a rock or log. Thus, a 120 mm compression of the driver's side spring was considered and all previous weights continued to be present. Even without any safety multiplier, stresses with magnitudes above the yield strength are generated in the beams that have the spring load applied. This would mean that a spring displacement comprehended in the suspension travel would cause permanent deformation on the chassis. Consequently, those sections shall be reinforced and the load wider spread.

The final dynamic simulations, pendulum impact based, were carried based on ECE-R29-02 [8] and its 3 tests, Test A, B and C. In all cases, the rotational pendulum was considered to be a linear pendulum, hitting the structure with speed derived from the standard imposed energy and corresponding to the tangential speed that a real impactor would have at the collision point:

- During Test A, the stress values reached the rupture level on two beams and the displacement of the frontal plane was substantial. Under this test, the cab can not be considered certification worthy and further reinforcement, around the front occupant feet section, should be considered to ensure that the instrument panel and steering system do not collide with the front occupants.
- The opposite occurred with the A pillar test, Test B. The pillars are capable of withstanding the load, with resulting stresses below the tensile strength, and the deformation not big enough to enter in contact with the driver or front passenger.
- The final test, Test C, even though capable of bearing with the stresses caused by the two distinct loads, does deform significatively. Consequently, the allowance of the caused deformations is not certain and it is recommended to either increase the height of the cab by around 250 mm and/or change the geometry of the first roll bar to further enhance the vertical rigidity.

Table 10 presents the obtained validation results for the 5 different scenarios that the chassis was subjected to. In sum, the integrity of the chassis was not possible to assure with the simulations carried: statically, because of the limitation on the definition of the suspension anchoring points and dynamically due to the geometry of the certain parts of the cab.

Table 10. Test validation results

	Static		**ECE-R29-02**		
Test	Regular mission	Static bump	Test A	Test B	Test C
Validation	✓	x	x	✓	±

5.2 Future works

In the future, to reach a worthy iteration of the chassis to manufacture a full-scale operational prototype, along with the need of a final decision on all the components to equip and their mounting locations, the recommendations made about the reinforcement of the structure shall be employed. Furthermore, all the tests simulated resorting to FEM analysis shall be again performed not only with the complementary parts and location information and with, at least, their thereto blocks for the cab certification tests, but also with a better, ideally precise, definition of the suspension anchoring points.

An additional interesting and crucial study that could be conducted in a future occasion, which would require the final component selection, is the simulation of the behaviour of the truck when travelling in uneven terrain. For instance, using a harmonic road profile, to assess the natural frequency of the chassis and if, by any chance, it would start entering the resonance zone.

In final remark, some design options, such as the choice of the windscreen, may be reassessed to ensure that some current concerns may be mitigate.

References

[1] CEN - European Committee for Standardization, "EN 1846-1:2011 Firefighting and rescue service vehicles Nomenclature and designation," 2011.

[2] CEN - European Committee for Standardization, "EN 1846-2:2009+A1:2013 Firefighting and rescue service vehicles Common requirements. Safety and performance," 2013.

[3] CEN - European Committee for Standardization, "EN 1846-3:2013 Firefighting and rescue service vehicles Permanently installed equipment. Safety and performance," 2013.

[4] National Fire Protection Association, "NFPA 414 - Standard for Aircraft Rescue and Fire-Fighting Vehicles," 2007.

[5] ICAO - International Civil Aviation Organization, "Airport Services Manual - Part I - Rescue and Firefighting (Doc 9137P1)," 2015.

[6] Jacinto Marques de Oliveira, Sucrs, Lda, "Inovação," O Carapau Criativo, [Online]. Available: https://www.jacinto-lda.com/inovacao/. [Accessed March 2023].

[7] Jacinto Marques de Oliveira, Sucrs, Lda, "Fotos de Jacinto Marques de Oliveira, Sucrs, Lda," [Online]. Available: https://www.facebook.com/JacintoMO/photos. [Accessed April 2023].

[8] "Regulation No 29 of the Economic Commission for Europe of the United Nations (UN/ECE) — Uniform provisions concerning the approval of vehicles with regard to the protection of the occupants of the cab of a commercial vehicle [2019/1850]," 2019. [Online]. Available: http://data.europa.eu/eli/reg/2019/1850/oj.

[9] J.-l. Dupuy, H. Fargeon, M.-S. Nicolas, F. Pimont, J. Ruffault, M. Guijarro, C. Hernando, J. Madrigal and P. Fernandes, "Climate change impact on future wildfire danger and activity in southern Europe: a review," *Annals of Forest Science*, vol. 77, 2020.

[10] M. Rodrigues, À. Cunill Camprubí, R. Balaguer-Romano, C. J. Coco Megía, F. Castañares, J. Ruffault, P. M. Fernandes and V. Resco de Dios, "Drivers and implications of the extreme 2022 wildfire season in Southwest Europe," *Science of The Total Environment,* vol. 859, 2023.

[11] European Forest Fire Information System - EFFIS, "EFFIS Statistics Portal," 2023. [Online]. Available: https://effis.jrc.ec.europa.eu/apps/effis.statistics/. [Accessed March 2023].

[12] European Environment Agency, "Burnt area in European countries," November 2021. [Online]. Available: https://www.eea.europa.eu/data-and-maps/daviz/burnt-forest-area-in-five-4/#tab-chart_5.

[13] J. San-Miguel-Ayanz, T. Durrant, R. Boca, G. Libertà, A. Branco, D. de Rigo, D. Ferrari, P. Maianti, T. Artés Vivancos, H. Costa, F. Lana, P. Löffler, D. Nuijten, A. Christofer Ahlgren and T. Leray, "Forest Fires in Europe, Middle East and North Africa 2017," 2018.

[14] ICNF - Instituto da Conservação da Natureza e das Florestas, "8.º Relatório Provisório De Incêndios Rurais," 2022.

[15] Copernicus Atmosphere Monitoring Service, “Europe’s summer wildfire emissions highest in 15 years,” 6 September 2022. [Online]. Available: https://atmosphere.copernicus.eu/europes-summer-wildfire-emissions-highest-15-years. [Accessed March 2023].

[16] Copernicus Atmosphere Monitoring Service, “Q&A - wildfires,” [Online]. Available: https://atmosphere.copernicus.eu/qa-wildfires. [Accessed March 2023].

[17] National Oceanic and Atmospheric Administration, “Wildfire climate connection,” 8 August 2022. [Online]. Available: https://www.noaa.gov/noaa-wildfire/wildfire-climate-connection. [Accessed March 2023].

[18] H. Costa, D. de Rigo, G. Libertà, T. Houston Durrant and J. San-Miguel-Ayanz, “European wildfire danger and vulnerability in a changing climate: towards integrating risk dimensions,” Publications Office of the European Union, Luxembourg, 2020.

[19] C. F. T. Young, Fires, Fire engines, and Fire Brigades: with a History of Manual and Steam Fire Engines, London: Lockwood & CO, 1866.

[20] Fire Safety Advice Centre, “History of Fire Extinguishers,” 15 March 2011. [Online]. Available: https://www.firesafe.org.uk/history-of-fire-extinguishers/.

[21] F. E. Dayton, Two Thousand Years of Steam, Frederick A. Stokes company, 1925.

[22] E. Peterson, “Who Invented the Steam Engine?,” 19 March 2014. [Online]. Available: https://www.livescience.com/44186-who-invented-the-steam-engine.html.

[23] R. H. Thurston, A History of the Growth of the Steam-Engine, Cornell University Press, 1878.

[24] C. T. Lira, “Brief History of the Steam Engine,” 21 May 2013. [Online]. Available: https://www.egr.msu.edu/~lira/supp/steam/index.htm.

[25] Science Museum Group, “First Steam Fire Engine Constructed in England AD 1830”.

[26] Science Museum Group, “Water colour drawing (scale 1:12) of first steam fire engine constructed in the U.S. of North America,” 1840.

[27] A. D. Amaro, “O socorro em Portugal - Organização, formação e cultura de segurança nos corpos de bombeiros, no quadro da Protecção Civil,” [Doctoral dissertation, Universidade do Porto], 2009.

[28] J. Guerrinha, Bombeiros de Gouveia (1904-2004), 2004.

[29] Mercedes-Benz Group Media, “1888: Gottlieb Daimler files patent application for first gasoline-powered fire-fighting pump,” 1 January 2008. [Online]. Available: https://group-media.mercedes-benz.com/marsMediaSite/ko/en/9913578.

[30] Mercedes-Benz Group Media, “1906: The world’s first fire-fighting pump powered by a gasoline engine goes into operation,” 30 October 2006. [Online]. Available: https://group-media.mercedes-benz.com/marsMediaSite/ko/en/9910179.

[31] Cummins News, “1937 Stutz... America's First Diesel-Powered Fire Truck,” [Online]. Available: https://columbus.in.us/wp-content/uploads/2016/09/1937-stutz-info.pdf. [Accessed April 2023].

[32] "Electric Fire-engine System Patent Artwork," [Online]. Available: https://web.archive.org/web/20170323143035/http://www.sirenworld.com/misc/patents/firefighting-patents/electric-fire-engine-system-patent-artwork. [Accessed April 2023].

[33] "Wonderfull Fire Engine," *The Los Angeles Times,* p. 8, 11 May 1903.

[34] *The Camden Chronicle,* p. 2, 9 June 1899.

[35] "A Review of Current Progress in Electricity and its Pratical Applications," *Electrical World,* vol. 65, 1915.

[36] Maximize Market Research, "Fire Trucks Market – Growth, Trends, COVID-19 Impact and Forecasts (2022-2029)," January 2023.

[37] Mordor Intelligence, "Fire Truck Market - Growth, Trends, Covid-19 Impact, And Forecasts (2023 - 2028)," 2023.

[38] Market Research Future, "Fire Truck Market," April 2023.

[39] Mordor Intelligence, "Europe Fire Truck Market - Growth, Trends, Covid-19 Impact, And Forecasts (2023 - 2028)," 2023.

[40] Eurostat, "Fires in the EU call firefighters to the test," 09 August 2022. [Online]. Available: https://ec.europa.eu/eurostat/web/products-eurostat-news/-/ddn-20220809-1.

[41] Eurostat, "General government expenditure by function (COFOG)," [Online]. Available: https://ec.europa.eu/eurostat/databrowser/view/GOV_10A_EXP__custom_3112132/bookmark/table?lang=en&bookmarkId=93d61af6-244f-4e69-8d8d-f50adce2582d&page=time:2021. [Accessed April 2023].

[42] Instituto da Mobilidade e dos Transportes, "Legislação," [Online]. Available: https://www.imt-ip.pt/sites/IMTT/Portugues/Legislacao/Paginas/Legislacao.aspx. [Accessed April 2023].

[43] TugaFire, "Fotos de TugaFire," [Online]. Available: https://www.facebook.com/profile.php?id=100066552046103&sk=photos. [Accessed 2023 April].

[44] Rosenbauer, "New Products," [Online]. Available: https://www.everythingforthatmoment.com/en/new-products/. [Accessed March 2023].

[45] Magirus, "Deliveries," [Online]. Available: https://www.magirusgroup.com/de/en/serving-heroes/deliveries/. [Accessed March 2023].

[46] PowerBully, "Magirus FireBull," [Online]. Available: https://www.powerbully.com/en/home/track-carrier/magirus-firebull.html. [Accessed March 2023].

[47] PowerBully, "Track Carrier Chassis," [Online]. Available: https://www.powerbully.com/en/home/track-carrier/chassis.html. [Accessed March 2023].

[48] Iturri, "Forest Fire Fighting Truck," [Online]. Available: https://www.iturri.eu/en/products/firefighting?view=productcategory&id=5. [Accessed April 2023].

[49] Ziegler, “Products,” [Online]. Available: https://www.ziegler.de/en/frontpage. [Accessed April 2023].

[50] Advanced Design Solution, “Driveline Systems for High Mobility Vehicles - Brochure,” 2023. [Online]. Available: http://www.ads-cz.com/ADS_BROCHURE_2023.pdf.

[51] CEN - European Committee for Standardization, “EN 1993-1-1 Eurocode 3: Design of steel structures - Part 1-1: General rules and rules for buildings,” 2005.

[52] F. Yang and M. Veljkovic, “Damage Model Calibration for S275 and S690 steels,” *XII Conference on Steel and Composite Construction,* pp. 262-271, 2019.

[53] W. Ramberg and W. R. Osgood, “Description of stress-strain curves by three parameters,” *National Advisory Committee for Aeronautics - Technical Note,* no. 902, 1943.

[54] H. N. Hill, “Determination of stress-strain relations from "offset" yield strength values,” *National Advisory Committee for Aeronautics - Technical Note,* no. 927, 1944.

[55] R. C. Rice, J. L. Jackson, J. Bakuckas and S. Thompson, “Metallic Materials Properties Development and Sstandardization (MMPDS),” U.S. Department of Transportation - Federal Aviation Administration, 2003.

[56] M. Kamaya, “RambergeOsgood type stressestrain curve estimation using yield and ultimate strengths for failure assessments,” *International Journal of Pressure Vessels and Piping,* no. 137, pp. 1-12, 2016.

[57] A. S. Hall, A. R. Holowenko and H. G. Laughlin, Elementos orgânicos de máquinas, McGraw-Hill, 1981.

[58] CEN - European Committee for Standardization, “EN 13906-1: Cylindrical helical springs made from round wire and bar - Calculation and design - Part 1 : Compression springs,” 2013.

[59] Advanced Design Solution, “Product Specification - Independent Suspension Axle System - AX75,” [Online]. Available: http://www.ads-cz.com/AX75_v2.pdf. [Accessed May 2023].

[60] Government of Canada, “Natural Resources Canada - Canadian Forest Fire Weather Index (FWI) System,” [Online]. Available: https://cwfis.cfs.nrcan.gc.ca/background/summary/fwi. [Accessed March 2023].

[61] Instituto Português do Mar e da Atmosfera, “Perigosidade Meteorológica de Fogos Florestais - IPMA,” [Online]. Available: http://mf2.ipma.pt/about. [Accessed March 2023].

[62] S. H. Lo, “Finite element mesh generation andadaptive meshing,” *Progress in Structural Engineering and Materials,* no. 4, pp. 381-399, 2002.

ANNEX A: FWI - Fire Weather Index

The Fire Weather Index System, CFFWIS, is an assessment metric of the fire danger influenced by the meteorological conditions and was developed by the Canadian Forest Service. Five factors enter on the algorithm to reach the Fire Weather Index, FWI, value: Fine Fuel Moisture Code (FFMC), Duff Moisture Code (DMC) and the Drought Code (DC), when regarding the fuel moisture and, Initial Spread Index (ISI) and Buildup Index (BUI), when considering the fire behaviour. The first parameter, FFMC, serves as a measure of the cured fine fuels and litter (0.25 kg/m^2), easily ignited, moisture content, DMC, homologous represents the humidity quantity on moderate duff layers and medium-size woody material (5 kg/m^2). Lastly on water content, DC, a useful indicator of seasonal drought effects on forest fuels expresses the moisture of deep and compact organic layers (25 kg/m^2). For the fire behaviour layer, ISI is based on the experienced wind and on the smaller sized fuel quality, rated by FFMC, and consists of the early spreading speed of a fire. Finally, BUI focuses more on the totalized quantity of fuel available [9, 60, 61].

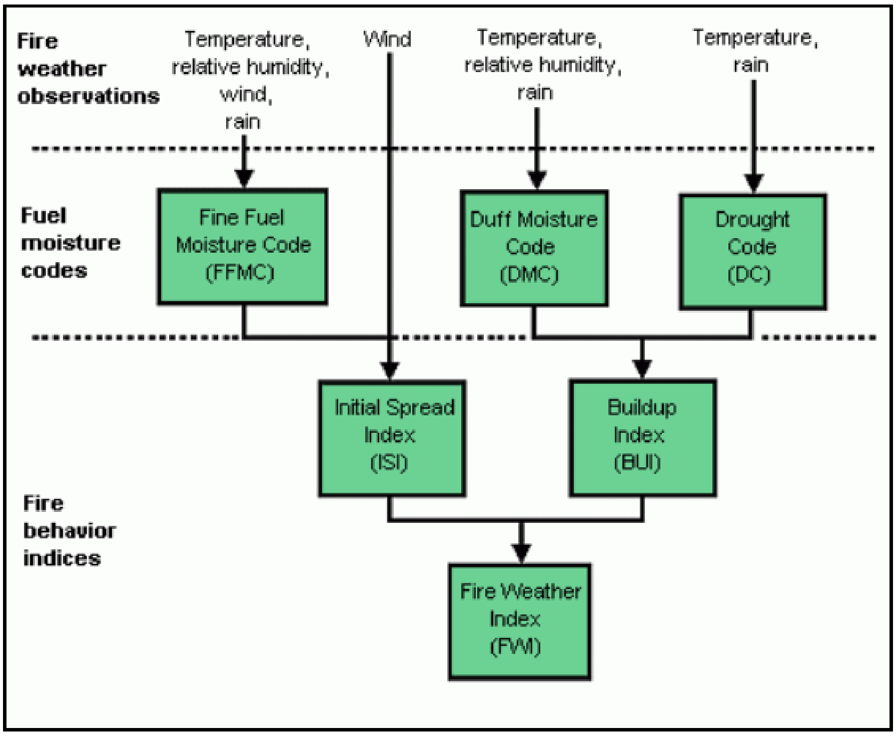

Figure 51. FWI determination flow chart [60].

Simplifying, the FWI value is computed taking into account consecutive daily observations of relative humidity, temperature, wind speed, and the accumulated 24-hour precipitation and their influence on the fuel moisture and fire behaviour, as seen in Figure 51. Furthermore, CFFWIS also includes the includes the Seasonal Severity Rating, SSR, which represents the fire management difficulty over a wildfire season and is the average value of the Daily Severity Rating, DSR, derived from the daily FWI rating and focused on the expected effort required for fire suppression [9, 60].

ANNEX B: Windscreen technical drawing

The available information for the Lusitano's windscreen, developed in a technology and innovation center upon Jacinto's request, is the following technical drawing, Figure 52.

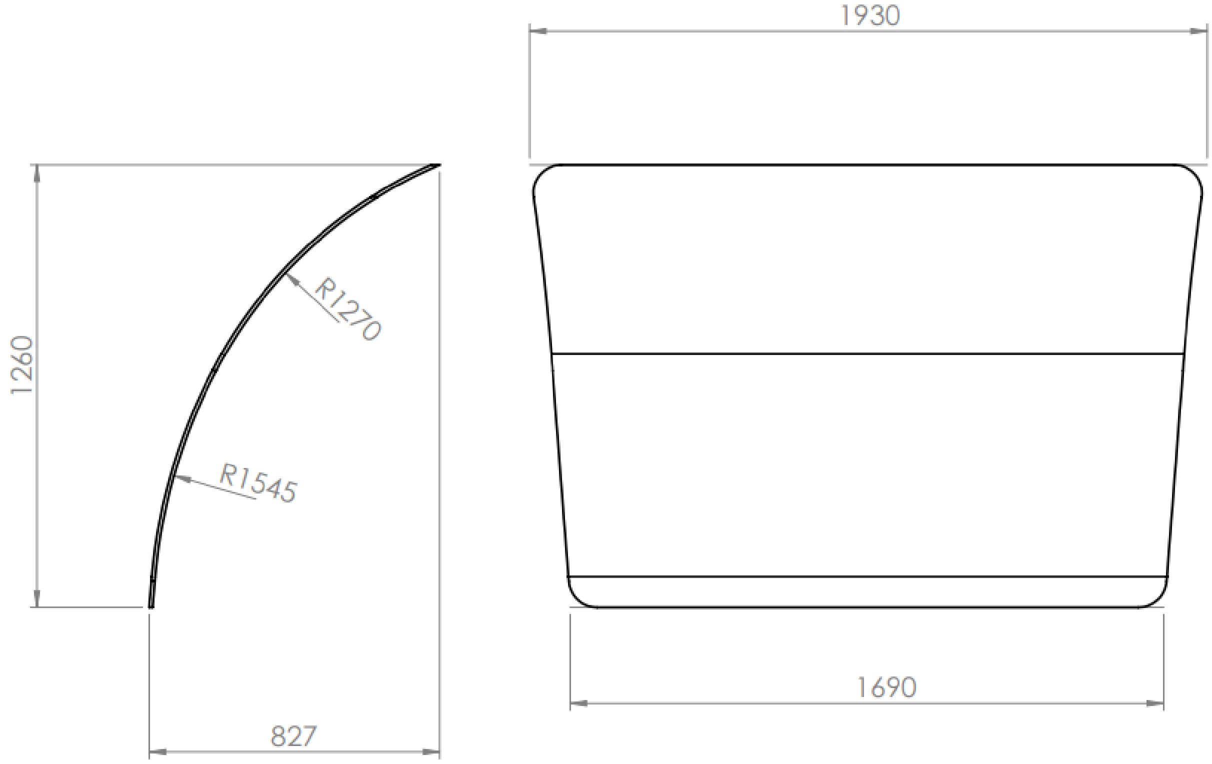

Figure 52. Lusitano's windscreen technical drawing.

ANNEX C: Beam sections used

The used beam sections are listed in Table 11 and all are made of S275 graded steel.

Table 11. Beam sections used

	Dimensions	**Section**
Circular (d x **t)**	60.3 x 2.9	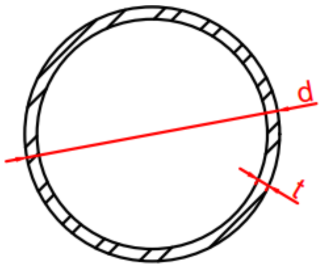
Squared (b x **t)**	40 x 4 50 x 3 60 x 3 100 x 4	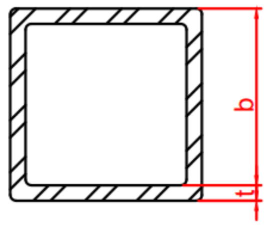
Rectangular (a x **b** x **t)**	60 x 40 x 3 100 x 40 x 3 100 x 40 x 3 100 x 60 x 3	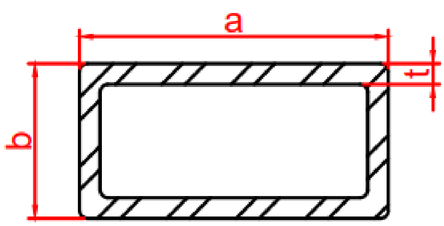

ANNEX D: True material properties

Table 12 presents the used plastic properties.

Table 12. Used true material plastic properties

Yield Stress	Plastic Strain
275	0
287.4114633	0.001233852
304.3023534	0.003905577
321.7914564	0.008163105
340.2334825	0.014801906
360.1601695	0.024926497
382.3534408	0.040022889
407.9431713	0.062018073
438.5361288	0.093300998
476.384007	0.136669096
524.6	0.195161662

ANNEX E: Convergence study

A FEM numerical analysis is fundamentally just a breakdown of a large continuum problem into smaller finite problems. This division and the accuracy of the obtained results is based on the mesh and the numbers of elements composing it. What is more the number os elements is governed by the number of nodes/seeds. In some cases, such as in problems with contact or large punctual loadings, it may even be beneficial to shrink the seed size locally, consequently increasing the number of elements, to ensure that the area has a greater definition. In essence, generally, a mesh can be considered as better as smaller the seed size is, in other words, as better as the higher the number of elements is [62].

For this reason, to obtain an admissible value for the number of elements that the mesh should have, a convergence study should be performed. This study is based on the multiple running of the same loading scenario simulation with different mesh refinements. The objective is to find the mesh with a sufficient number of elements, to achieve acceptable results, with the least CPU time needed.

For the current mesh under study, the first simulation of the static study is run several times with different seed sizes. The mesh properties, the maximum stress obtained, and the respective CPU time needed to compute the simulation with the distinct meshes is presented in Table 13 and plotted in Figure 53 and Figure 54, respectively.

Table 13. Mesh properties, max stress and CPU time

Seed size (mm)	No. Elements	Max Stress (MPa)	CPU time (s)
250	830	214.9	1.3
150	1 300	231.8	1.4
100	1 864	264.2	1.5
75	2 447	276.6	1.7
50	3 650	278.8	2.7
25	7 285	286.5	5
15	12 133	289.8	9.8
10	18 196	293.5	18.7
7.5	24 248	296.1	28.2
5	36 351	298.7	47.8
3	60 585	300.8	117.6
2	90 883	301.8	355.7
1.5	121 186	302.4	762.2
1	181 743	-	-

The final iteration with a 1 mm seed size mesh was not possible to finish in the numerous attempts tried, due to lack of memory on the computer used.

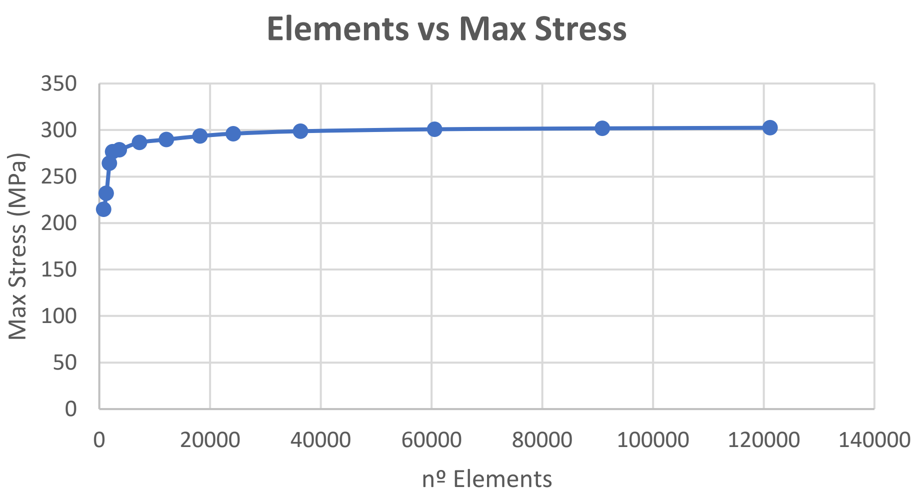

Figure 53. No. Elements vs Max Stress.

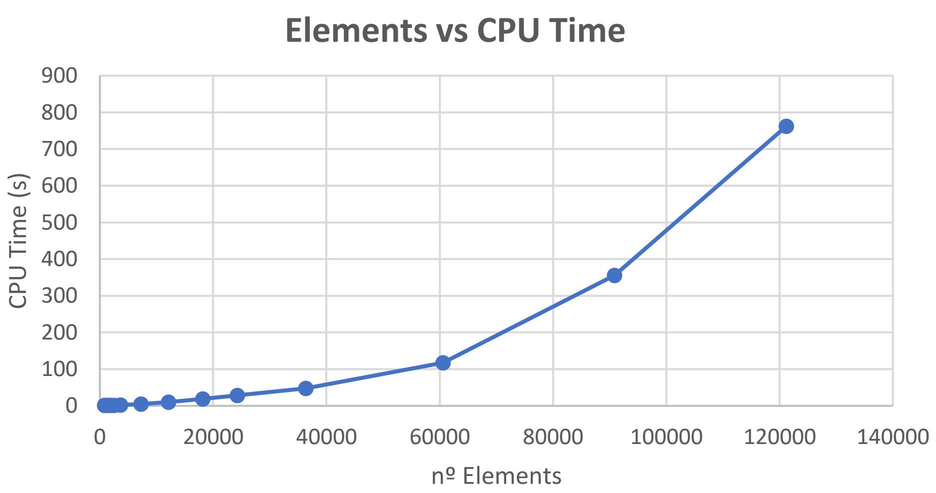

Figure 54. No. Elements vs CPU Time.

Hereby, it can be said that the last 3 iterations of the study, with the smallest seed size and the highest number of elements, were able to achieve similar maximum stress values. The deviation between the 1.5 mm mesh and the 3 mm and 2 mm mesh results is of 0.50% and 0.17%, respectively. Admissibly the results convergence is found, and the final mesh size shall be decided based on the computational time. Since the 1.5 mm mesh accounts to less than 13 minutes, this will be the final mesh size used.

ANNEX F: Simulation stop criteria - Test A

The evolution of the kinetic energy throughout the simulation is presented in Figure 55.

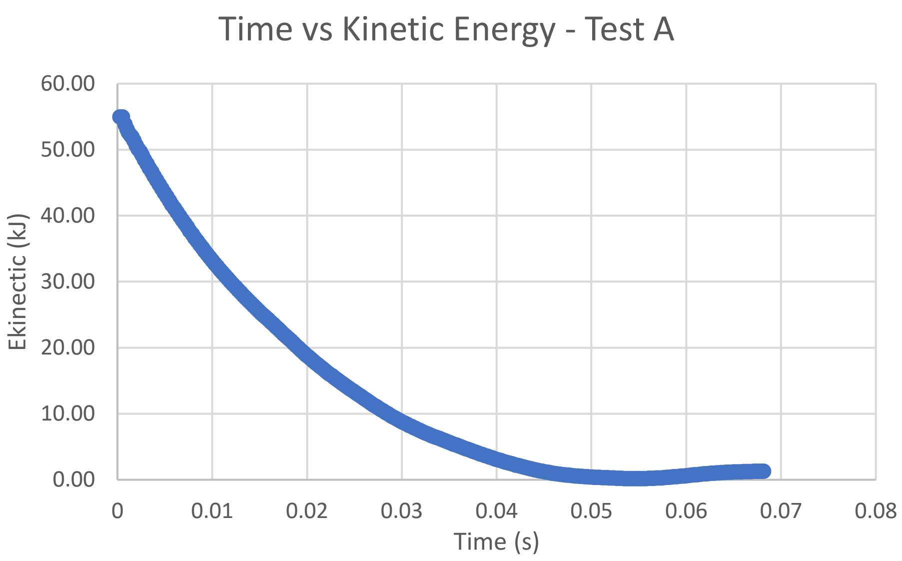

Figure 55. Simulation time vs kinetic energy - Test A.

To understand the inversion of the kinetic energy's progression, a greater focus is given after 0.0412755 s of simulation and represented in Figure 56.

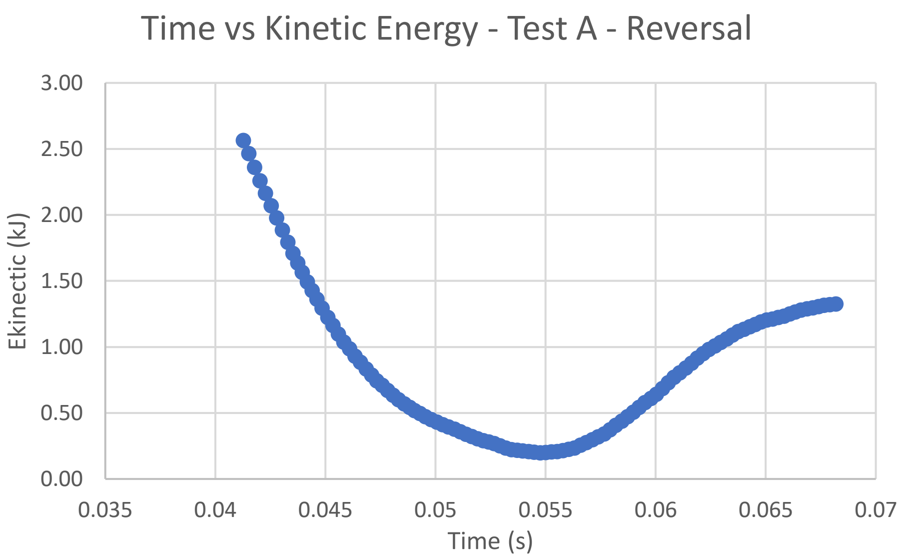

Figure 56. Simulation time vs kinetic energy - Test A - Reversal.

ANNEX G: Simulation stop criteria - Test B

The evolution of the kinetic energy throughout the simulation is presented in Figure 57.

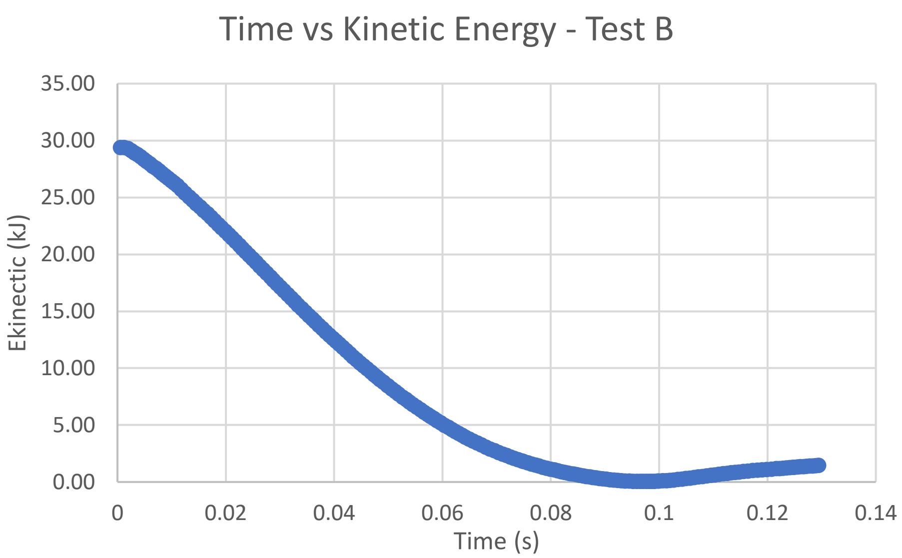

Figure 57. Simulation time vs kinetic energy - Test B.

To understand the inversion of the kinetic energy's progression, a greater focus is given after 0.0680269 s of simulation and represented in Figure 58.

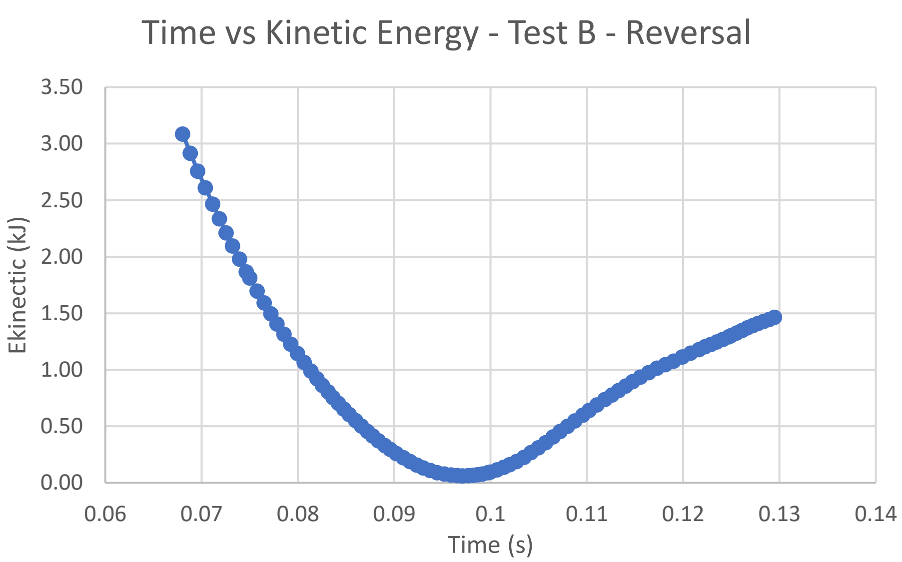

Figure 58. Simulation time vs kinetic energy - Test B - Reversal.